

Coordination corrected *ab initio* formation enthalpies

Rico Friedrich,^{1,2} Demet Usanmaz,^{1,2} Corey Oses,^{1,2} Andrew Supka,³ Marco Fornari,^{2,3}
Marco Buongiorno Nardelli,^{2,4} Cormac Toher,^{1,2} and Stefano Curtarolo^{2,5,6,*}

¹*Department of Mechanical Engineering and Materials Science,
Duke University, Durham, North Carolina 27708, USA*

²*Center for Materials Genomics, Duke University, Durham, North Carolina 27708, United States*

³*Department of Physics and Science of Advanced Materials Program,
Central Michigan University, Mount Pleasant, Michigan 48859, USA*

⁴*Department of Physics and Department of Chemistry,
University of North Texas, Denton, TX 76203, USA*

⁵*Materials Science, Electrical Engineering, Physics and Chemistry, Duke University, Durham NC, 27708, USA*

⁶*Fritz-Haber-Institut der Max-Planck-Gesellschaft, 14195 Berlin-Dahlem, Germany*

(Dated: April 9, 2019)

The correct calculation of formation enthalpy is one of the enablers of *ab-initio* computational materials design. For several classes of systems (*e.g.* oxides) standard density functional theory produces incorrect values. Here we propose the “Coordination Corrected Enthalpies” method (CCE), based on the number of nearest neighbor cation-anion bonds, and also capable of correcting relative stability of polymorphs. CCE uses calculations employing the Perdew, Burke and Ernzerhof (PBE), Local Density Approximation (LDA) and Strongly Constrained and Appropriately Normed (SCAN) exchange correlation functionals, in conjunction with a quasiharmonic Debye model to treat zero-point vibrational and thermal effects. The benchmark, performed on binary and ternary oxides (halides), shows very accurate room temperature results for all functionals, with the smallest mean absolute error of 27 (24) meV/atom obtained with SCAN. The zero-point vibrational and thermal contributions to the formation enthalpies are small and with different signs — largely cancelling each other.

I. INTRODUCTION

The accurate prediction of the thermodynamic stability of a compound — crucial in computational materials design [1] — mostly relies on the calculation of the formation enthalpy: the enthalpy change with respect to elemental reference phases. Using Density Functional Theory (DFT), the formation energy, neglecting pressure-volume contributions, is routinely computed *ab initio*. For systems where elements and compounds are metallic, *i.e.* chemically similar, accurate results are usually obtained by using standard (semi)local approximations to DFT [2, 3]. They include the Local Density Approximation (LDA) [4, 5] or the Generalized Gradient Approximation (GGA), for instance PBE [6]. In this way, formation energies for millions of metal alloys have already been calculated in materials databases such as AFLOW [7–10], the Materials Project [11, 12] and OQMD [13, 14].

When the compound and the elements have a different chemical character, as for example in case of oxides, nitrides or sulfides, the situation is less favorable. For oxides, the compound is typically an ionic insulator while the elements are metals or semiconductors and a diatomic gas. When comparing to experimental enthalpies [15–18], standard approximations of DFT lead to Mean Absolute Errors (MAEs) of the order of several hundred meV/atom. For reaction energies between binary and ternary oxides, within a similar chemical realm, a smaller average error of about 24–35 meV/atom has been observed [19].

Correcting DFT. Different attempts have been made to calculate more accurate formation energies *ab initio*.

A modified version of PBE was proposed by Sarmiento-Pérez *et al.* [20]: three functional parameters were optimized, improving results by about a factor of two. The hybrid functional HSE06 yields only a slight improvement for transition metal oxides [21]. The recently developed Strongly Constrained and Appropriately Normed (SCAN) meta-generalized-gradient approximation [22] has an accuracy limited to about 100 meV/atom [23, 24].

Beyond DFT. Non self-consistent EXact eXchange plus Random Phase Approximation (EXX+RPA) calculations can lead to more accurate formation energies by about a factor of two to three compared to PBE [25, 26]. The renormalized adiabatic PBE method improves the results based on RPA for 19 main group and two transition metal oxides by about a factor of two [27]. A Bayesian Error Estimation Functional (mBEEF) systematically improves PBE results reaching an MAE of about 120 meV/atom for a test set of 24 compounds [28]. Applying a correction method on top of the functional could reduce the MAE to 90 meV/atom, which is 20–60 meV/atom less than if the correction is applied on top of other functionals. Unfortunately, such computationally expensive approaches are not suitable for screening large materials sets and do not, in general, reach the necessary chemical accuracy of 1 kcal/mol (\approx 40 meV/atom).

Empirical corrections. Several empirical correction schemes have been established for formation energies calculated with DFT by comparing to experimentally measured formation enthalpies. Wang *et al.* [29] suggested an oxygen correction of 1.36 eV per O₂ to be subtracted from formation energies calculated with PBE. The approach was extended to H₂, N₂, F₂ and Cl₂ for different functionals [30]. For sulfides, a different correction is found depending on whether the anion is S²⁻ or S₂²⁻ [31]. Jain

* stefano@duke.edu

et al. suggested an empirical scheme for mixing GGA and GGA+ U calculations to compute formation enthalpies for compounds containing transition metal elements [32]. An MAE of 45 meV/atom was achieved for a test set of 49 ternary oxides with respect to experimental values [32]. A local environment dependent GGA+ U method based on the GGA/GGA+ U mixing scheme was also developed [33]. It introduced significantly more parameters and achieved an MAE of 19 meV/atom for a test set of 52 transition metal oxides. In the Fitted Elemental-phase Reference Energies (FERE) method [34, 35], element specific corrections were used to optimize the error cancellation when calculating total energy differences between chemically dissimilar materials. Corrected formation energies calculated for a test set of 55 ternary compounds gave an MAE of 48 meV/atom [35]. In conclusion, existing correction schemes and advanced theoretical approaches do not, in general, reach an accuracy of the order of the thermal energy at room temperature (~ 25 meV) for formation enthalpies.

Topological corrections: coordination corrected enthalpies. Here, we propose a physically motivated correction scheme — Coordination Corrected Enthalpies (CCE), based on the number of bonds between each cation and surrounding anions. Compared to previous approaches, it leads to systematically more accurate results. The smallest MAE of 27 (24) meV/atom for a test set of ternary oxides (halides) is reached when starting from SCAN calculations. Contrary to earlier approaches, the ansatz also allows correction of the relative stability of polymorphs with different number of cation-anion bonds.

The article mainly focuses on oxides because of: **i.** high technological relevance, **ii.** abundance of experimental thermochemical data, especially for ternary oxides and **iii.** generally low error bars of the experimental values allowing accurate corrections and predictions. Calculated room temperature formation enthalpies for a set of 79 binary and 71 ternary oxides are presented employing the three main approximations to the DFT exchange-correlation functional: LDA, PBE and SCAN.

In other schemes, temperature effects have been completely neglected [32, 34, 35], or room temperature experimental values were interpolated to 0 K using a Debye model parameterized with the measured room temperature heat capacities and entropies [19, 33]. Here, the thermal contributions to the formation enthalpy are calculated via a quasiharmonic Debye model [36–40]. Our approach includes the contribution due to zero-point vibrational energies.

The methodology of calculating coordination corrected room temperature formation enthalpies is presented in Section II. The DFT derived and CCE results are discussed in Section III. Conclusions are summarized in Section IV. Additional comparisons are given in Appendices A to

D. Tables with structure data, values of the corrections, of calculated, corrected and experimental formation enthalpies/energies as well as the vibrational contributions are listed in Appendix F.

II. METHODOLOGY

Room temperature formation enthalpies. The formation enthalpy includes contributions due to the pressure-volume term (*e.g.* for O₂). The formation energy takes into account only internal energy contributions. The formalism, introduced for oxides, works equivalently for other polar systems.

From DFT, an approximate formation energy $\Delta_f E^{0,\text{DFT}}$ of an oxide $A_{x_1}B_{x_2}\dots O_{x_n}$ at zero T and p , without zero-point vibrational energies, can be calculated:

$$\Delta_f E_{A_{x_1}\dots O_{x_n}}^{0,\text{DFT}} = U_{A_{x_1}\dots O_{x_n}}^{0,\text{DFT}} - \left[\sum_{i=1}^{n-1} x_i U_i^{0,\text{DFT}} + \frac{x_n}{2} U_{O_2}^{0,\text{DFT}} \right], \quad (1)$$

where $U_{A_{x_1}\dots O_{x_n}}^{0,\text{DFT}}$, $U_i^{0,\text{DFT}}$ and $U_{O_2}^{0,\text{DFT}}$ are the total energies of the compound per formula unit, the i -element reference phase per atom, and O₂, respectively, and x_1, \dots, x_n are stoichiometries.

The tabulated experimentally measured standard formation enthalpy at the reference temperature $T_r=298.15$ K, $\Delta_f H^{\circ,T_r,\text{exp}}$, corresponds to:

$$\Delta_f H_{A_{x_1}\dots O_{x_n}}^{\circ,T_r,\text{exp}} = H_{A_{x_1}\dots O_{x_n}}^{\circ,T_r} - \left[\sum_{i=1}^{n-1} x_i H_i^{\circ,T_r} + \frac{x_n}{2} H_{O_2}^{\circ,T_r} \right], \quad (2)$$

where $H_{A_{x_1}\dots O_{x_n}}^{\circ,T_r}$, H_i°,T_r} and $H_{O_2}^{\circ,T_r}$ are the standard enthalpies of the compound per formula unit, the i -element reference phase per atom and O₂, respectively, all at T_r .

Using $H = U + pV$ and neglecting the pV terms for the compound and the elements (less O₂), the formation enthalpy becomes:

$$\Delta_f H_{A_{x_1}\dots O_{x_n}}^{\circ,T_r,\text{exp}} \approx U_{A_{x_1}\dots O_{x_n}}^{T_r} - \left[\sum_{i=1}^{n-1} x_i U_i^{T_r} + \frac{x_n}{2} H_{O_2}^{\circ,T_r} \right]. \quad (3)$$

Generally, neglecting pV is a very good approximation: pressures are small and the molar volumes of condensed systems are typically three orders of magnitude smaller than gases — the contribution to the formation enthalpy is expected to be well below 1 meV/atom.

Writing the total energies and the standard enthalpy of O₂ at T_r as the value at 0 K plus the difference between T_r and 0 K, and separating the zero-point vibrational energy for each system, gives:

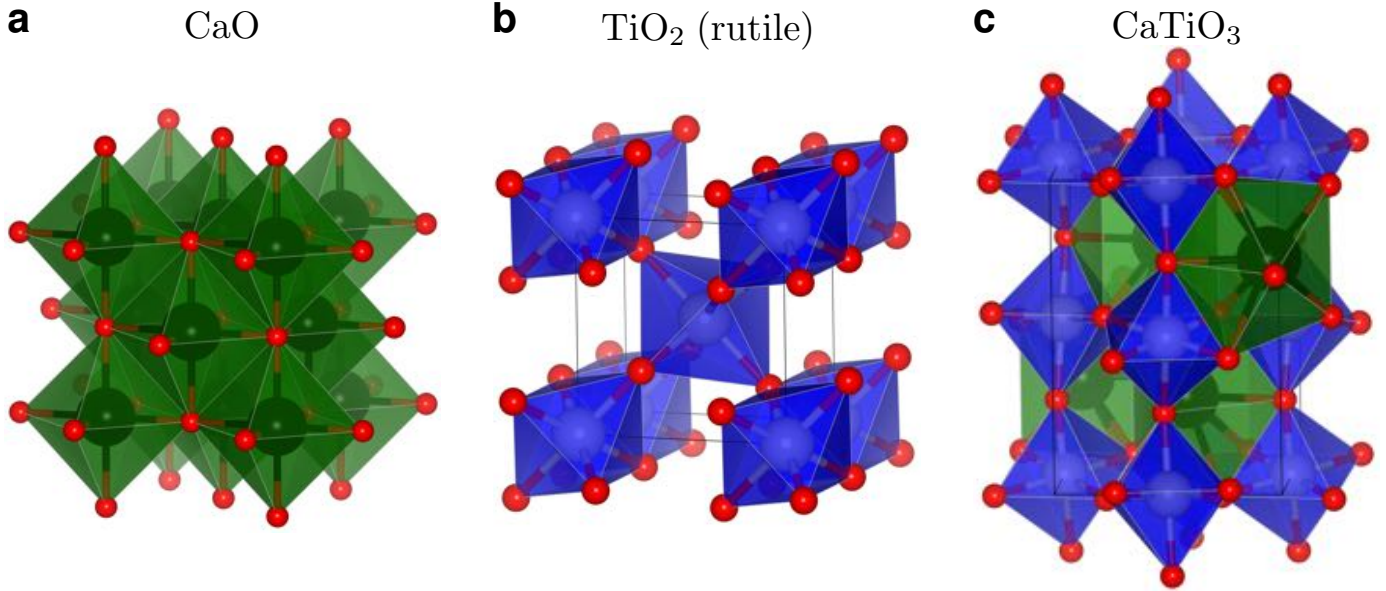


FIG. 1. **Coordination change.** Crystal structures of (a) CaO, (b) rutile TiO₂, and (c) CaTiO₃ (perovskite). The coordination polyhedra of Ca and Ti are shown green and blue, respectively. Note: Ca is six-fold (octahedrally) coordinated with oxygen in CaO and eight-fold coordinated in CaTiO₃, requiring coordination corrections. Colors: Ca black, Ti light gray, and O red [41].

$$\begin{aligned} \Delta_f H_{A_{x_1} \dots O_{x_n}}^{o, T_r, \text{exp}} &\approx U_{A_{x_1} \dots O_{x_n}}^0 + U_{A_{x_1} \dots O_{x_n}}^{\text{ZP}} + \Delta U_{A_{x_1} \dots O_{x_n}}^{T_r - 0\text{K}} - \left[\sum_{i=1}^{n-1} x_i (U_i^0 + U_i^{\text{ZP}} + \Delta U_i^{T_r - 0\text{K}}) + \frac{x_n}{2} (U_{O_2}^0 + U_{O_2}^{\text{ZP}} + \Delta H_{O_2}^{o, T_r - 0\text{K}}) \right] \\ &\approx \Delta_f E_{A_{x_1} \dots O_{x_n}}^0 + \Delta_f E_{A_{x_1} \dots O_{x_n}}^{\text{ZP}} + \Delta_f H_{A_{x_1} \dots O_{x_n}}^{\text{TC}} \approx \Delta_f H_{A_{x_1} \dots O_{x_n}}^{o, T_r, \text{cal}}, \end{aligned} \quad (4)$$

where $U_{A_{x_1} \dots O_{x_n}}^{\text{ZP}}$, U_i^{ZP} and $U_{O_2}^{\text{ZP}}$ are the zero-point vibrational energies of the compound, the i -element reference and O₂, respectively. $\Delta_f H_{A_{x_1} \dots O_{x_n}}^{o, T_r, \text{cal}}$ stands for the calculated standard formation enthalpy at T_r . The terms are:

$$\Delta_f E_{A_{x_1} \dots O_{x_n}}^0 \equiv U_{A_{x_1} \dots O_{x_n}}^0 - \left[\sum_{i=1}^{n-1} x_i U_i^0 + \frac{x_n}{2} U_{O_2}^0 \right] \quad (5)$$

is the internal energy contribution excluding vibrational effects;

$$\Delta_f E_{A_{x_1} \dots O_{x_n}}^{\text{ZP}} \equiv U_{A_{x_1} \dots O_{x_n}}^{\text{ZP}} - \left[\sum_{i=1}^{n-1} x_i U_i^{\text{ZP}} + \frac{x_n}{2} U_{O_2}^{\text{ZP}} \right] \quad (6)$$

collects all Zero-Point (ZP) contributions;

$$\Delta_f H_{A_{x_1} \dots O_{x_n}}^{\text{TC}} \equiv \Delta U_{A_{x_1} \dots O_{x_n}}^{T_r - 0\text{K}} - \left[\sum_{i=1}^{n-1} x_i \Delta U_i^{T_r - 0\text{K}} + \frac{x_n}{2} \Delta H_{O_2}^{o, T_r - 0\text{K}} \right] \quad (7)$$

is the overall Thermal Contribution (TC).

The internal energy contribution to $\Delta_f H_{A_{x_1} \dots O_{x_n}}^{o, T_r, \text{exp}}$ can be identified with $\Delta_f E_{A_{x_1} \dots O_{x_n}}^{0, \text{DFT}}$ calculated with DFT according

to Eq. (1). The pressure dependence is negligible at the standard value of 1 bar.

For the thermal contribution, the internal energy differences between 0 K and T_r are almost entirely due to vibrations. The quantity is estimated by using the AFLOW Automatic GIBBS Library (AGL) via a quasiharmonic Debye model [36–40] with default parameters (28 strained structures, 1% lattice strain increments [39]). The approach is tested by comparing the calculated internal energy difference between 0 K and T_r with experimental enthalpy differences as illustrated in Fig. A.6 (Appendix A), indicating good agreement for both compounds and references.

The AGL calculations also provide a zero-point vibrational energy, which is used to treat the zero-point contribution. Notably, *e.g.* for BeO the energy is calculated to be 0.11 eV/atom for all three functionals, which agrees *exactly* with the value reported in Ref. [42] obtained from more expensive phonon calculations. In the rest of the article, the sum of the zero-point and thermal contributions is denoted as the vibrational contribution.

For O₂, the enthalpy difference between 0 K and T_r can be estimated from a perfect diatomic gas with five degrees of freedom where the bond-stretching vibrational mode is not excited at T_r , leading to 90 meV/O₂ [43]. The value

agrees exactly with the tabulated enthalpy difference from the NIST-JANAF thermochemical tables [16]. For F_2 , Cl_2 , BF_3 and SiF_4 , the enthalpy differences from NIST-JANAF corresponding to 91, 95, 121 and 159 meV are taken, respectively. The zero-point vibrational energy of O_2 is calculated, using the experimental oxygen vibrational frequency of 1580.1932 cm^{-1} [16], to be 98 meV/ O_2 . For F_2 , Cl_2 , BF_3 and SiF_4 , the calculated zero-point energies are 55, 35, 339 and 346 meV. Similarly, for Hg the total energy at 0 K is calculated for the low temperature rhombohedral structure, with the zero-point vibrational energy obtained from AGL. The experimental enthalpy difference from 0 K to T_r of 97 meV/ Hg atom from the NIST-JANAF tables [16], including fusion at 234.29 K, is used to account for thermal effects.

Coordination corrected enthalpies scheme. The remaining deviation between calculated and measured room temperature formation enthalpies is almost entirely due to the internal energy contribution $\Delta_f E_{A_{x_1}\dots O_{x_n}}^{0,\text{DFT}}$ obtained with DFT. Compounds with strong polar bonds are chemically different from elements — mostly metallic plus a diatomic gas. As already noted by Lany [34] and Stevanović *et al.* [35], this leads to an incomplete error cancellation when calculating total energy differences — standard semilocal functionals do not allow calculation of accurate total energies.

Since a reliable description of the bonding in a material is central for capturing its properties, it seems reasonable to assume in first approximation that DFT makes errors *per bond*. As such, the CCE scheme considers the number of nearest neighbor bonds (coordination number) formed between the cation and oxygen. The approach enables accounting for coordination changes, as illustrated in Fig. 1 for the case of CaO , rutile TiO_2 and perovskite $CaTiO_3$. For the binary oxides, Ca is six-fold (octahedrally) coordinated by O in the rocksalt structure of CaO , while Ti is six-fold in rutile TiO_2 . For Ti , the coordination number remains the same in $CaTiO_3$, but the number of nearest neighbor Ca - O bonds changes to eight. The phenomenon is quite common for several elements when going from binary to ternary oxides, and can be captured within CCE.

The corrections per bond $\delta H_{A-O}^{A+\alpha}$ are extracted from the deviation between the calculated and experimental formation enthalpies of binary oxides $A_{x_1}O_{x_2}$ for each functional:

$$\Delta_f H_{A_{x_1}O_{x_2}}^{\circ,T_r,\text{cal}} - \Delta_f H_{A_{x_1}O_{x_2}}^{\circ,T_r,\text{exp}} = x_1 N_{A-O} \delta H_{A-O}^{A+\alpha}, \quad (8)$$

where N_{A-O} is the number of nearest neighbor A - O bonds of element A in oxidation state $+\alpha$. CCE is constructed to be dependent on $+\alpha$: the energetic position of the bonding states and hence also the correction are expected to be oxidation state specific. In AFLOW, oxidation numbers can be determined by a Bader analysis [44, 45], while ensuring that the sum over all atoms equals zero. When counting bonds for distorted or low symmetry environments, a length variation up to 0.5 Å is allowed. After trying different tolerances, this value is found to lead

to the best results. In the case of $CaTiO_3$ (see Fig. 1(c)) the nearest neighbor Ca - O bond length varies between 2.36 and 2.69 Å for the relaxed PBE structure.

As mentioned before, DFT errors do not only originate from the inaccurate treatment of the bonding in the compound, but also from the lack of error cancellation with the different reference phases. CCE corrections per bond implicitly include those of the elemental references — for a given bonded pair of atoms, reference phases are constant and the lack of error cancellation is then “absorbed” into corrections per bond. It especially applies to the molecular O_2 reference, for which the atomization energy is known to be poorly described in DFT [29].

The energy corrections extracted from binary oxides are then applied to the test-set of ternary oxides $A_{x_1}B_{x_2}O_{x_3}$ to calculate the corrected formation enthalpies:

$$\Delta_f H_{A_{x_1}B_{x_2}O_{x_3}}^{\circ,T_r,\text{cor}} = \Delta_f H_{A_{x_1}B_{x_2}O_{x_3}}^{\circ,T_r,\text{cal}} - \sum_{i=1,2} x_i N_{i-O} \delta H_{i-O}^{i+\alpha}, \quad (9)$$

where N_{i-O} is the number of nearest neighbor bonds between the cation i -species and oxygen.

Compared to other approaches [29, 32–35], it is important to note that at fixed composition, CCE is capable of correcting the relative stability of polymorphs with different coordination numbers.

Comparisons are performed with a quasi-FERE approach following the ideas of Refs. [34, 35]. A least-squares problem for all binary oxides in the fitting set is solved for the element specific corrections $\delta H_i^{\text{qFERE}}$:

$$\Delta_f H_{A_{x_1}O_{x_2}}^{\circ,T_r,\text{exp}} = \Delta_f H_{A_{x_1}O_{x_2}}^{\circ,T_r,\text{cal}} - \sum_{i=1,2} x_i \delta H_i^{\text{qFERE}}. \quad (10)$$

The corrections are then added to the calculated reference enthalpies used to calculate the corrected formation enthalpies. Contrary to the original FERE [34, 35], here **i.** no Hubbard- U term is used, **ii.** only oxides are considered in the fitting set, **iii.** the corrections are determined and applied with respect to the calculated room temperature formation enthalpies rather than DFT formation energies, and **iv.** in part different experimental data are used.

Principal thermodynamic considerations. There is also another *caveat*. Corrections depending linearly on the concentration (like the previously proposed renormalization of the chemical potential of one or more species) are equivalent to tilting the whole Gibbs landscape, and might — in some cases — lead to thermodynamic paradoxes. For example, consider the case of non-ideal activity *vs.* concentration, differing from the Raoult’s law with a negative(positive) deviation at low(high) concentration [46]. Any linear interpolation tends to balance the deviations and erroneously correct the chemical potential by decreasing its non-ideal behavior. This is a rare scenario. Yet, phase diagrams having a very-high monotectoid and very-low eutectoid do exist, and the accuracy of calculated

critical temperatures would be reduced with unappropriately corrected enthalpies. The problem can be solved only by including more information in the DFT correction, introducing non linearity and/or considering topology and oxidation states like in the case of CCE.

Ab-initio calculations. Calculations are performed using the AFLOW framework [7–10, 45, 47–50] leveraging the Vienna *Ab-initio* Simulation Package (VASP) [51, 52] with projector-augmented-wave pseudopotentials [53] of version 5.4. The exchange-correlation functionals LDA [4, 5], PBE [6] and SCAN [22] are employed. The parameters of the structural relaxation and static calculations largely follow the AFLOW Standard for entries from the ICSD library [47] with the internal VASP precision set to ACCURATE. No Hubbard-*U* term is used, and for the elements Li, Be, Na and W, pseudopotentials with the labels Li, Be, Na_pv and W_sv are taken, respectively. For calculating total energy differences between a compound and its references, the kinetic energy cutoff is set to be 40% larger than the highest value recommended among all pseudopotentials for the compound but to at least 560 eV (oxygen cutoff). For magnetic systems, spin-polarized calculations are performed with all possible ferro-, ferri- and antiferromagnetic configurations initialized for five different sizes of the induced magnetic moments in the primitive unit cell. For computational efficiency, for Ti_4O_7 , Ti_5O_9 and Ti_6O_{11} , only four different ferromagnetic configurations were initialized. The final magnetic state with the lowest total energy is considered for the formation enthalpy.

All room temperature structures are obtained from the AFLOW-ICSD online library [7, 9, 10, 47]. The selection is based on the structure information in the Kubaschewski *et al.* tables [15]. If it is insufficient, it is taken from the Springer Materials database [54]. The ICSD numbers, space groups and Pearson symbols are listed in Table A.V and A.VI (Appendix F). Space-groups and Pearson symbols are calculated with AFLOW-SYM [55]. For SiO_2 , both the α -quartz (space group $P3_121$ #152; Pearson symbol hP9; AFLOW prototype A2B_hP9_152_c_a [49, 50, 56]) and α -cristobalite ($P4_12_12$ #92; tP12; A2B_tP12_92_b_a [49, 50, 57]) prototypes are considered. TiO_2 is calculated in the rutile ($P4_2/mnm$ #136; tP6; A2B_tP6_136_f_a [49, 50, 58]) and anatase ($I4_1/amd$ #141; tI12; A2B_tI12_141_e_a [49, 50, 59]) structures. Al_2SiO_5 is represented in the kyanite ($P\bar{1}$ #2; aP32) and andalusite ($Pnmm$ #58; oP32) structures. $CaSiO_3$ is treated as wollastonite ($P\bar{1}$ #2; aP30) and pseudowollastonite ($C2/c$ #15; mS60). For O_2 , F_2 , Cl_2 , BF_3 and SiF_4 , a $10 \times 10 \times 10 \text{ \AA}^3$ cubic box is used, the intermolecular bond length is relaxed until the forces are smaller than 10 meV/ \AA , and the Brillouin zone is sampled only at the Γ -point.

Selection of experimental data. The accuracy of experimental data used is crucial. For oxides and halides, several reliable thermochemical libraries do exist, and here, we rely on the collections of Kubaschewski *et al.* [15], NIST-JANAF [16], Barin [17] and NBS [18].

For the validation of the experimental room tempera-

ture enthalpies, a procedure similar to Hautier *et al.* [19] is applied. Each $\Delta_f H^{\circ, T_r, \text{exp}}$ of Kubaschewski *et al.* [15] is first compared to the values from the NIST-JANAF database [16], which is believed to be the most accurate [19]. If the deviation exceeds 5 meV/atom, the value from Ref. [16] is used. For the oxides with no corresponding entry in NIST-JANAF, the formation enthalpies are compared with the Barin ones. If the values differ by more than 10 meV/atom, Barin's $\Delta_f H^{\circ, T_r, \text{exp}}$ is used. $NaCrO_2$ is an exception: the Kubaschewski formation enthalpy is taken, since the Barin value deviates by 0.15 eV/atom from the Kubaschewski and NBS data. Both Hautier *et al.* [19] and Aykol & Wolverton [33] used the $\Delta_f H^{\circ, T_r, \text{exp}}$ from Kubaschewski and obtained good agreement with the calculated reaction energies and formation enthalpies — this would not have been possible with the Barin value. In general, the NBS collection might not be considered as a suitable source for comparisons: When compared to all others, it exhibits several examples with significant deviations (Appendix B). This might be at least partially due to the special consistency requirements within NBS [18]. Oxides from Kubaschewski with no corresponding formation enthalpy in Barin are therefore excluded. For halides, the procedure is relaxed for $NaBF_4$ and Na_2SiF_6 due to the scarcity of experimental data for polar ternaries other than oxides. In these two cases, the Kubaschewski formation enthalpy is taken, which could only be verified by NBS.

III. RESULTS AND DISCUSSION

A. Room temperature DFT+AGL results

The difference between calculated DFT+AGL and experimental room temperature formation enthalpies for 79 binary and 71 ternary oxides for the three functionals employed are illustrated in Fig. 2. The vibrational (zero-point + thermal) contribution is shown in the lower panels of panels (a,b). MAEs are included in Table I. The calculated formation enthalpies for each functional, together with the experimental values, are included in Tables A.VII and A.IX (Appendix F). The vibrational, zero-point and thermal contributions are listed in Tables A.XII and A.XIV.

Vibrational contribution. In general the vibrational term is very small (lower panels of Fig. 2(a,b)), and decreases with increasing atomic number of the non-O elements. The maximum value of 23 (23) meV/atom is reached for Al_2O_3 (kyanite- Al_2SiO_5) with SCAN. The minimum of -22 (-4) meV/atom occurs for HgO ($PbWO_4$) with LDA (PBE and SCAN). For HgO , this is due to the heat of fusion of Hg being about 24 meV/atom at 234.29 K [16]. On average, the absolute vibrational value for binaries (ternaries) is very small: 5, 7 and 6 (7, 9 and 8) meV/atom for PBE, LDA and SCAN, respectively, due to partial cancellations of the zero-point and thermal contributions (Section III of Appendix C provides

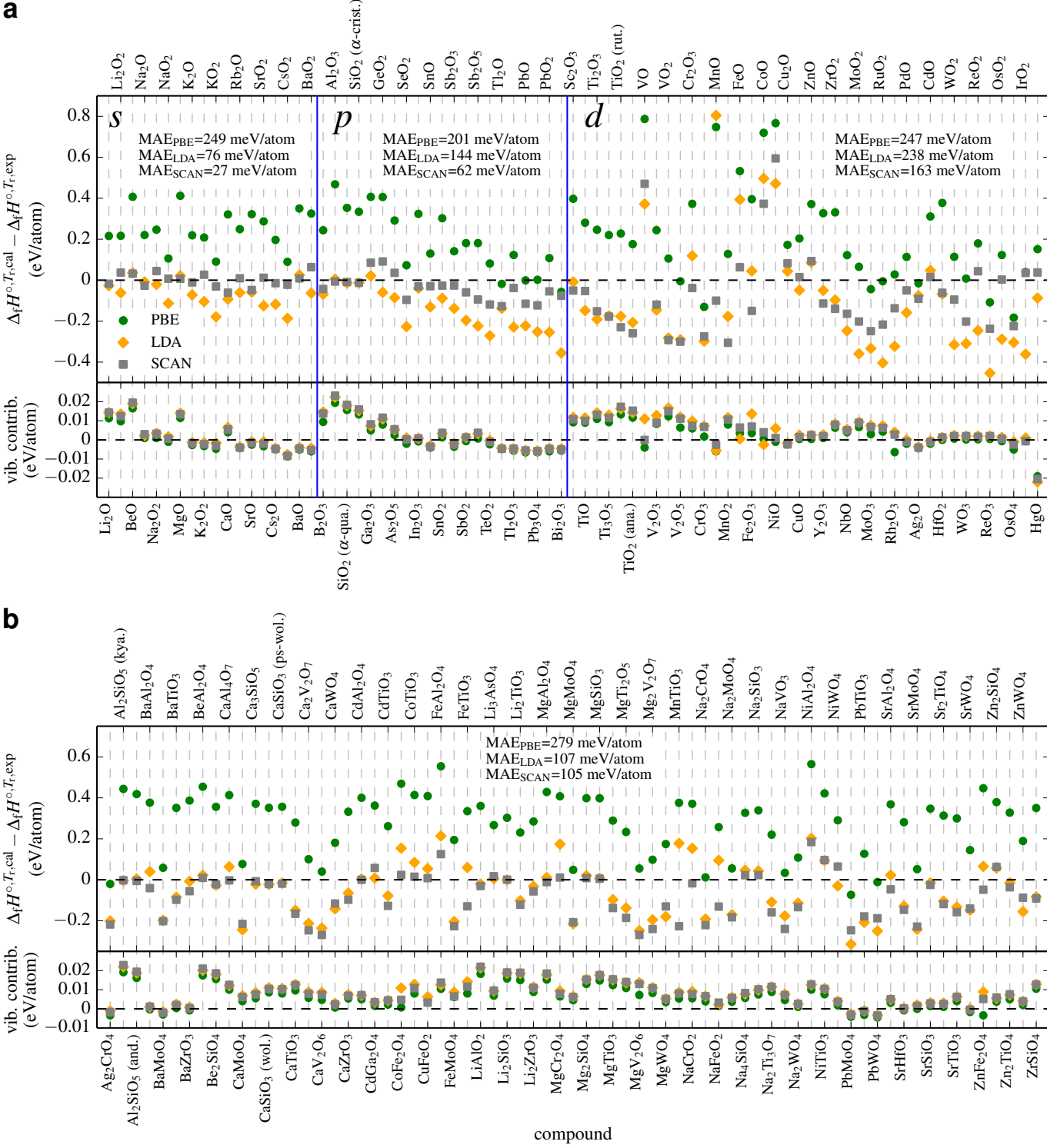


FIG. 2. Uncorrected enthalpies. Differences between calculated (Eq. (4)) and experimental room temperature formation enthalpies of binary oxides ((a) upper panel) and vibrational (zero-point + thermal) contribution to the calculated formation enthalpy ((a) lower panel). Vertical blue lines separate the different l -blocks with respect to the position of the non-O element of the compound in the periodic table. Differences between calculated and experimental room temperature formation enthalpies of ternary oxides ((b) upper panel) and vibrational contribution to the calculated formation enthalpy ((b) lower panel).

additional insights). Unless stated otherwise, our PBE, LDA and SCAN formation enthalpies include vibrational contributions, which, despite the often negligible values,

consistently improve the MAEs of LDA and SCAN for binaries and ternaries by 2-5 meV/atom (Table I). For PBE, the MAE increases when including the vibrational value

TABLE I. MAEs of uncorrected and corrected enthalpies. MAEs of the uncorrected room temperature DFT+AGL, CCE and quasi-FERE corrected formation enthalpies for both binary and ternary oxides with respect to the experimental values. The numbers in brackets denote the MAEs of the calculated and corrected formation energies when no vibrational contribution is considered. Note that for the binary oxides CCE is basically exact by construction. All values in meV/atom.

calculation type	binaries			ternaries		
	PBE	LDA	SCAN	PBE	LDA	SCAN
plain DFT+AGL	235 (234)	176 (178)	105 (107)	279 (273)	107 (109)	105 (110)
CCE corrected	5 (5)	4 (4)	3 (3)	38 (38)	29 (30)	27 (27)
quasi-FERE corrected	53 (54)	44 (44)	48 (48)	43 (42)	35 (36)	44 (44)

— most likely an artifact for the functional having the largest errors.

Comparison of calculated and experimental results. In Figure 2(a), the compounds are grouped according to the *l*-block of the non-O element in the periodic table. Materials are ordered with respect to increasing atomic number of the non-O element. PBE tends to underestimate the formation enthalpy leading to the largest deviations from the experimental values (MAE 235 meV/atom). Both LDA and SCAN show an increasingly better performance with total MAEs of 176 and 105 meV/atom, respectively. The findings are in agreement with previous reports [23, 35] including similar compounds. LDA was found to systematically yield better formation energies than PBE [34] for a much smaller set of 13 (9 binary, 4 ternary) oxides.

Results indicate a pronounced dependence on the *l*-character of the non-O element. For *s*-oxides, SCAN gives very accurate formation enthalpies with an MAE of 27 meV/atom, with LDA and PBE showing increasing deviations. For *p*-oxides, all functionals display a decreasing trend in $\Delta_f H^{\circ,T_r,\text{cal}}$ with respect to $\Delta_f H^{\circ,T_r,\text{exp}}$ with increasing atomic number of the non-O species, the trend being weakest for SCAN. Spin-orbit coupling could be the culprit, although often the effect largely cancels out when calculating formation energies [35, 60]. Instead, the trend might be caused by an increasing degree of covalency. MAEs for the combined set of all *s*- and *p*- (main group) oxides of 223, 113 and 46 meV/atom are obtained for PBE, LDA and SCAN, respectively. The values are in good agreement with Ref. [23], where a largely similar set of main group oxides was investigated. For transition metal, *i.e.* *d*-oxides, all functionals show large errors of several hundred meV/atom, with SCAN having the smallest MAE of 163 meV/atom. For the ternary oxides, deviations similar to the binaries are shown in Fig. 2(b): MAEs are 279, 107 and 105 meV/atom for PBE, LDA and SCAN.

Further improvements on a semilocal DFT level might be difficult considering that SCAN already fulfills all known constraints required for the exact functional [22]. A promising direction might be provided by the recently developed size-extensive self-interaction correction scheme [61–64] potentially leading to more accurate formation enthalpies.

B. Coordination corrected enthalpies

This section compares the two correction schemes described in the Methods section: CCE and the quasi-FERE approach. The oxygen correction introduced by Wang *et al.* [29] is not considered as it shows a strong dependency on the fitting set when *p*-oxides are included (see Appendix D).

CCE uses the deviation between calculated and experimental room temperature formation enthalpies of single-valence binary oxides to obtain corrections per cation-O bond for each functional. They are then applied to the calculated formation enthalpies of ternary and mixed-valence binary oxides. The quasi-FERE method uses the binary data to obtain element specific corrections, optimizing the systematic error cancellation between the total energies/enthalpies of the references with respect to the compound [34, 35].

Corrected binary results. For the binary fit set, CCE gives almost exact solutions, as indicated by the small MAEs of 5, 4 and 3 meV/atom for PBE, LDA and SCAN (Table I). The corrections per bond are included in Table II and in Table A.VII (Appendix F). The quality is not surprising: the scheme is constructed to reproduce the experimental formation enthalpies of the single-valence binary oxides. The few other cases include mixed-valence compounds, multiple polymorphs at the same composition and per- as well as superoxides, leading to non-zero MAE for the binary set (Table I) and allowing assessment of CCE reliability. For SbO₂, the corrections obtained from Sb₂O₃ and Sb₂O₅ are used. Pb₃O₄ is refined based on PbO and PbO₂, and for Ti₃O₅ the corrections from Ti₂O₃ and TiO₂ (rutile) are taken. For SiO₂ (α -cristobalite) and TiO₂ (anatase), the $\delta H_{A-O}^{A+\alpha}$ determined from SiO₂ (α -quartz) and TiO₂ (rutile) are applied, respectively. The results are included in Table A.VII (Appendix F). For all cases, the corrected values agree well with the experimental data — typically within 20 meV/atom — and a maximum systematic deviation of about 50 meV/atom is observed for Pb₃O₄.

The per- and superoxides cannot be corrected exactly, since their structure incorporates bonds between the cation and O, as well as an internal O-O bond. The values are corrected based on the assumption that for the cation-O bond the correction of the normal (O²⁻) oxide can be taken, and the O-O bond correction is transferable

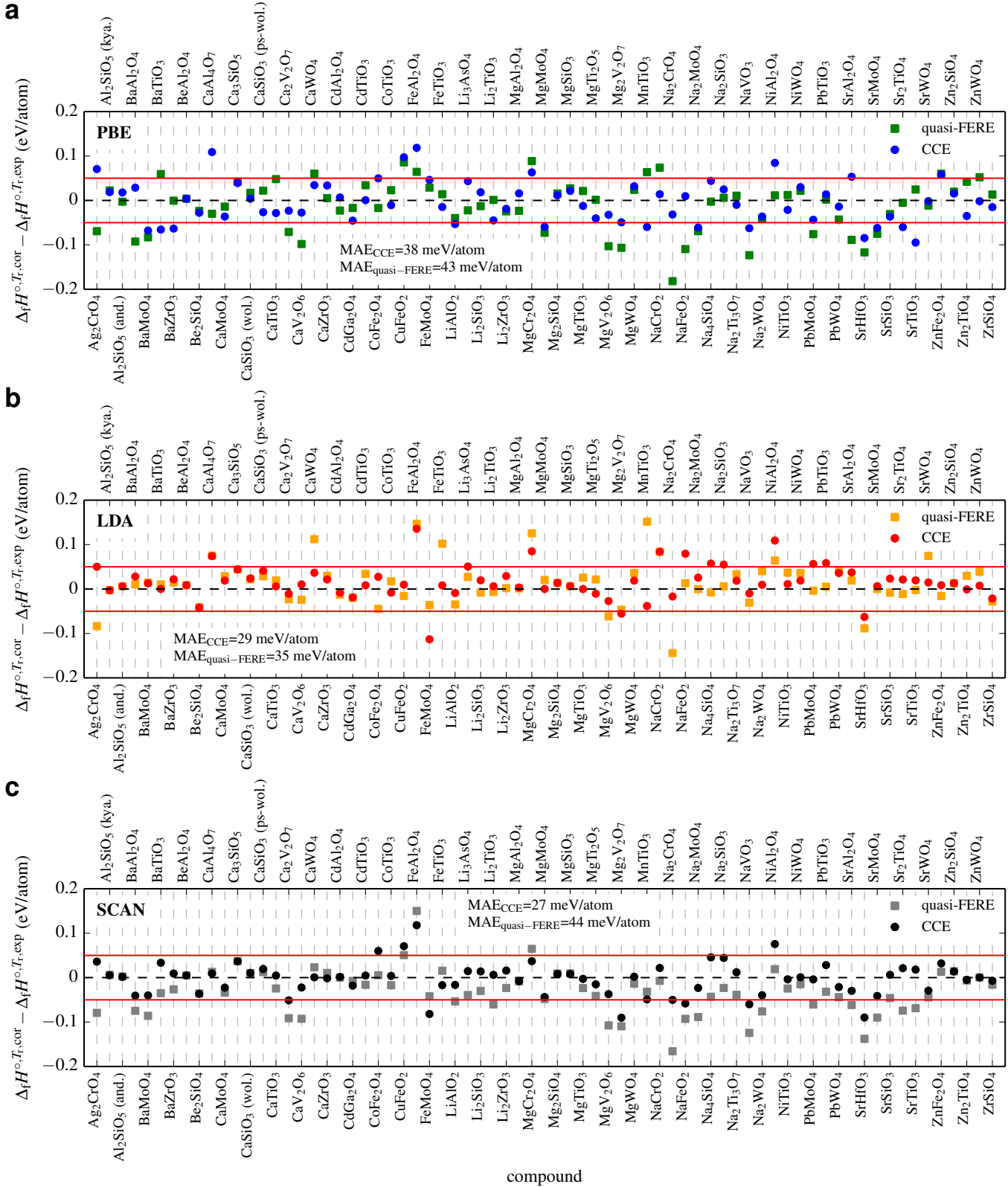


FIG. 3. Corrected enthalpies. Differences between corrected and experimental room temperature formation enthalpies of the test set of 71 ternary oxides for the CCE and quasi-FERE correction schemes on top of PBE (a), LDA (b) and SCAN (c). Note the different energy scale compared to Fig. 2. The red lines at ± 50 meV/atom indicate the typical MAE of previous correction schemes [32, 35].

between (su)peroxides: O-O correction for peroxides is

obtained from Li_2O_2 ; the O-O correction for superoxides

is derived from KO_2 . The two values are listed in Table A.VII (Appendix F). All other per- and superoxides are corrected based on these values. In general, the procedure leads to good agreement with experiment, and the largest absolute deviation occurs for the corrected PBE value of NaO_2 : 124 meV/atom (the absolute deviations for LDA and SCAN are 17 and 45 meV/atom, respectively).

For quasi-FERE, MAEs of 53, 44 and 48 meV/atom for PBE, LDA and SCAN are obtained for the binary fit set. They well agree with the MAE of 54 meV/atom reported for the original FERE in Ref. [35] using PBE for the fit set of binary compounds. Our calculations indicate that even better agreement is obtainable when using LDA or SCAN in the DFT calculations.

FERE tends to yield large deviations if multivalent p -oxides such as SnO , SnO_2 , Sb_2O_3 , SbO_2 , Sb_2O_5 , Tl_2O , Tl_2O_3 , PbO , PbO_2 and Pb_3O_4 are considered [35]. Indeed, for these systems, errors for the quasi-FERE corrected values partly exceeding 100 meV/atom are observed, in agreement with Ref. [35]. CCE circumvents the problem through its explicit dependence on the oxidation state of the cation according Eq. (8).

Corrected ternary results. The differences between CCE and quasi-FERE corrected and experimental room temperature formation enthalpies are displayed in Fig. 3 for the test set of 71 ternary oxides calculated with PBE

TABLE II: **CCE corrections per bond.** Corrections per bond $\delta H_{A-\text{O}}^{A+\alpha}$ of the CCE method for each cation species A in oxidation states $+\alpha$ obtained from calculated room temperature formation enthalpies of binary oxides. The numbers in brackets denote the corrections derived from the calculated DFT formation energies when no vibrational contribution is considered. The corrections for Si and Ti in oxidation state +4 are obtained from α -quartz and rutile, respectively. All corrections in eV/bond.

cation species A	$+\alpha$	$\delta H_{A-\text{O}}^{A+\alpha}$ PBE+AGL	$\delta H_{A-\text{O}}^{A+\alpha}$ (PBE)	$\delta H_{A-\text{O}}^{A+\alpha}$ LDA+AGL	$\delta H_{A-\text{O}}^{A+\alpha}$ (LDA)	$\delta H_{A-\text{O}}^{A+\alpha}$ SCAN+AGL	$\delta H_{A-\text{O}}^{A+\alpha}$ (SCAN)
Li	+1	0.0809	(0.0766)	-0.0100	(-0.0154)	-0.0065	(-0.0118)
Be	+2	0.2035	(0.1953)	0.0180	(0.0083)	0.0160	(0.0060)
B	+3	0.2030	(0.1952)	-0.0572	(-0.0693)	-0.0357	(-0.0472)
Na	+1	0.0826	(0.0823)	-0.0033	(-0.0043)	-0.0101	(-0.0113)
Mg	+2	0.1373	(0.1335)	0.0072	(0.0025)	0.0023	(-0.0023)
Al	+3	0.1950	(0.1869)	0.0020	(-0.0073)	-0.0028	(-0.0124)
Si (α -qua.)	+4	0.2648	(0.2530)	-0.0098	(-0.0233)	-0.0070	(-0.0208)
K	+1	0.0821	(0.0830)	-0.0269	(-0.0263)	-0.0041	(-0.0035)
Ca	+2	0.1070	(0.1057)	-0.0308	(-0.0332)	-0.0203	(-0.0222)
Sc	+3	0.1656	(0.1618)	-0.0034	(-0.0083)	-0.0212	(-0.0257)
Ti	+2	0.1169	(0.1131)	-0.0619	(-0.0667)	-0.0221	(-0.0265)
Ti	+3	0.1025	(0.0980)	-0.0796	(-0.0855)	-0.0633	(-0.0688)
Ti (rut.)	+4	0.1138	(0.1072)	-0.0882	(-0.0965)	-0.1150	(-0.1237)
V	+2	0.2623	(0.2637)	0.1240	(0.1203)	0.1568	(0.1568)
V	+3	0.1018	(0.0984)	-0.0608	(-0.0661)	-0.0498	(-0.0531)
V	+4	0.0528	(0.0467)	-0.1413	(-0.1497)	-0.1462	(-0.1537)
V	+5	-0.0037	(-0.0082)	-0.2033	(-0.2118)	-0.2101	(-0.2179)
Cr	+3	0.1553	(0.1528)	0.0495	(0.0454)	-0.0159	(-0.0189)
Cr	+6	-0.1305	(-0.1323)	-0.2980	(-0.3053)	-0.2745	(-0.2813)
Mn	+2	0.2492	(0.2513)	0.2682	(0.2700)	-0.0333	(-0.0325)
Mn	+4	0.0640	(0.0600)	-0.0885	(-0.0943)	-0.1528	(-0.1582)
Fe	+2	0.1775	(0.1763)	0.1312	(0.1310)	0.0210	(0.0188)
Fe	+3	0.1648	(0.1633)	0.0187	(0.0130)	-0.0625	(-0.0655)
Co	+2	0.2398	(0.2397)	0.1655	(0.1662)	0.1243	(0.1230)
Ni	+2	0.2555	(0.2558)	0.1572	(0.1552)	0.1982	(0.1980)
Cu	+1	0.1293	(0.1310)	0.0328	(0.0340)	0.0618	(0.0635)

(panel (a)), LDA (panel (b)) and SCAN (panel (c)). MAEs are included in Table I and the formation enthalpies are listed in Tables A.IX and A.XI (Appendix F). The importance of using *ab-initio* data as input for CCE is discussed in Appendix E. CCE predicts accurate results for almost all ternary compounds: MAE is 38, 29 and 27 meV/atom with PBE, LDA and SCAN, respectively. Compared to plain DFT+AGL, the errors are decreased by about a factor of 4-7. The mean deviations are significantly smaller than 45 and 48 meV/atom predicted by the GGA/GGA+ U mixing and FERE corrections of Refs. [32] and [35]. For the quasi-FERE method on the same set of compounds, MAEs of 43, 35 and 44 meV/atom are obtained for the corrected values of PBE, LDA and SCAN [65]. CCE consistently yields more accurate results than quasi-FERE for all three functionals. The MAEs of CCE are slightly larger than the 19 meV/atom of the local environment dependent GGA+ U method [33]. The latter scheme, however, uses about a factor two more parameters and is constructed for transition metal compounds. On the contrary CCE is applicable to all systems. CCE is simpler and more intuitive.

The largest single absolute deviation over the whole set is also higher for the quasi-FERE method — 182, 152 and 166 meV/atom for PBE (Na_2CrO_4), LDA (MnTiO_3) and SCAN (Na_2CrO_4) — compared to CCE — 118, 135 and 118 meV/atom for PBE, LDA and SCAN (always FeAl_2O_4).

TABLE II. (*continued*)

cation species <i>A</i>	$+\alpha$	$\delta H_{A-O}^{A+\alpha}$ PBE+AGL	$\delta H_{A-O}^{A+\alpha}$ (PBE)	$\delta H_{A-O}^{A+\alpha}$ LDA+AGL	$\delta H_{A-O}^{A+\alpha}$ (LDA)	$\delta H_{A-O}^{A+\alpha}$ SCAN+AGL	$\delta H_{A-O}^{A+\alpha}$ (SCAN)
Cu	+2	0.1018	(0.1015)	-0.0245	(-0.0258)	0.0075	(0.0068)
Zn	+2	0.1858	(0.1853)	0.0433	(0.0423)	0.0468	(0.0455)
Ga	+3	0.2034	(0.2009)	0.0105	(0.0068)	0.0427	(0.0386)
Ge	+4	0.2030	(0.1992)	-0.0300	(-0.0357)	0.0457	(0.0397)
As	+5	0.2039	(0.2022)	-0.0599	(-0.0636)	0.0251	(0.0212)
Se	+4	0.0730	(0.0750)	-0.2267	(-0.2277)	-0.0960	(-0.0963)
Rb	+1	0.0934	(0.0950)	-0.0229	(-0.0215)	0.0035	(0.0049)
Sr	+2	0.1073	(0.1082)	-0.0195	(-0.0192)	-0.0160	(-0.0155)
Y	+3	0.1363	(0.1358)	-0.0209	(-0.0219)	-0.0474	(-0.0483)
Zr	+4	0.1419	(0.1393)	-0.0416	(-0.0451)	-0.0597	(-0.0631)
Nb	+2	0.0610	(0.0593)	-0.1235	(-0.1263)	-0.0820	(-0.0845)
Mo	+4	0.0327	(0.0292)	-0.1797	(-0.1843)	-0.1008	(-0.1053)
Mo	+6	-0.0440	(-0.0470)	-0.3335	(-0.3410)	-0.2490	(-0.2558)
Ru	+4	-0.0027	(-0.0048)	-0.2020	(-0.2057)	-0.1085	(-0.1118)
Rh	+3	0.0115	(0.0141)	-0.1347	(-0.1363)	-0.0572	(-0.0583)
Pd	+2	0.0568	(0.0578)	-0.0793	(-0.0793)	-0.0250	(-0.0245)
Ag	+1	-0.0115	(-0.0083)	-0.0568	(-0.0540)	-0.0683	(-0.0653)
Cd	+2	0.1037	(0.1042)	0.0158	(0.0162)	0.0050	(0.0053)
In	+3	0.1349	(0.1353)	-0.0163	(-0.0167)	-0.0127	(-0.0130)
Sn	+2	0.0650	(0.0670)	-0.0653	(-0.0638)	-0.0148	(-0.0130)
Sn	+4	0.1512	(0.1505)	-0.0442	(-0.0460)	-0.0133	(-0.0153)
Sb	+3	0.1177	(0.1207)	-0.1150	(-0.1135)	-0.0218	(-0.0198)
Sb	+5	0.1056	(0.1052)	-0.1304	(-0.1323)	-0.0551	(-0.0573)
Te	+4	0.0610	(0.0630)	-0.2035	(-0.2033)	-0.0893	(-0.0885)
Cs	+1	0.0983	(0.1008)	-0.0588	(-0.0567)	-0.0073	(-0.0050)
Ba	+2	0.1167	(0.1183)	0.0085	(0.0098)	0.0028	(0.0042)
Hf	+4	0.1617	(0.1617)	-0.0290	(-0.0296)	-0.0263	(-0.0269)
W	+4	0.0570	(0.0567)	-0.1575	(-0.1587)	-0.0473	(-0.0483)
W	+6	0.0052	(0.0050)	-0.2063	(-0.2078)	-0.1347	(-0.1362)
Re	+4	0.0898	(0.0897)	-0.1230	(-0.1242)	0.0218	(0.0212)
Re	+6	-0.0722	(-0.0727)	-0.3027	(-0.3040)	-0.1582	(-0.1597)
Os	+4	0.0613	(0.0617)	-0.1438	(-0.1443)	0.0015	(0.0012)
Os	+8	-0.2288	(-0.2225)	-0.3805	(-0.3793)	-0.2803	(-0.2773)
Ir	+4	0.0198	(0.0202)	-0.1808	(-0.1813)	0.0177	(0.0180)
Hg	+2	0.1515	(0.1700)	-0.0870	(-0.0650)	0.0375	(0.0580)
Tl	+1	-0.0090	(-0.0065)	-0.0687	(-0.0665)	-0.0635	(-0.0612)
Tl	+3	0.0513	(0.0536)	-0.0955	(-0.0936)	-0.0159	(-0.0140)
Pb	+2	-0.0005	(0.0028)	-0.1115	(-0.1088)	-0.0575	(-0.0548)
Pb	+4	0.0538	(0.0568)	-0.1272	(-0.1250)	-0.0273	(-0.0250)
Bi	+3	-0.0286	(-0.0258)	-0.1775	(-0.1752)	-0.0381	(-0.0356)

TABLE III: CCE corrections per bond for halides. Corrections per bond $\delta H_{A-X}^{A+\alpha}$ ($X = F, Cl$) of the CCE method for each cation species *A* in oxidation states $+\alpha$ obtained from calculated room temperature formation enthalpies of binary halides. The numbers in brackets denote the corrections derived from the calculated DFT formation energies when no vibrational contribution is considered. The values below (above) the horizontal line refer to chlorides (fluorides). The corrections for B in oxidation state +3 and for Si in oxidation state +4 are obtained from the gaseous molecular systems BF_3 and SiF_4 . All corrections in eV/bond.

cation species <i>A</i>	$+\alpha$	$\delta H_{A-X}^{A+\alpha}$ PBE+AGL	$\delta H_{A-X}^{A+\alpha}$ (PBE)	$\delta H_{A-X}^{A+\alpha}$ LDA+AGL	$\delta H_{A-X}^{A+\alpha}$ (LDA)	$\delta H_{A-X}^{A+\alpha}$ SCAN+AGL	$\delta H_{A-X}^{A+\alpha}$ (SCAN)
Li	+1	0.0788	(0.0748)	0.0120	(0.0070)	-0.0482	(-0.0532)
Na	+1	0.0833	(0.0807)	0.0258	(0.0225)	-0.0473	(-0.0503)
K	+1	0.0718	(0.0702)	0.0083	(0.0060)	-0.0472	(-0.0490)
Be	+2	0.2073	(0.2008)	0.0563	(0.0480)	-0.1215	(-0.1300)
B	+3	0.2447	(0.2093)	0.1587	(0.1247)	-0.1640	(-0.1987)
Al	+3	0.2488	(0.2353)	0.0572	(0.0415)	-0.1208	(-0.1367)
Si	+4	0.3135	(0.2833)	0.1750	(0.1450)	-0.1525	(-0.1825)
Na	+1	0.1000	(0.0972)	0.0568	(0.0537)	0.0180	(0.0152)
K	+1	0.0938	(0.0913)	0.0488	(0.0460)	0.0168	(0.0142)
Ca	+2	0.1608	(0.1552)	0.0742	(0.0680)	0.0227	(0.0167)
Al	+3	0.1933	(0.1845)	0.0498	(0.0400)	0.0485	(0.0388)

TABLE III. (continued)

cation species <i>A</i>	$+ \alpha$	$\delta H_{A-X}^{A+\alpha}$ PBE+AGL	$\delta H_{A-X}^{A+\alpha}$ (PBE)	$\delta H_{A-X}^{A+\alpha}$ LDA+AGL	$\delta H_{A-X}^{A+\alpha}$ (LDA)	$\delta H_{A-X}^{A+\alpha}$ SCAN+AGL	$\delta H_{A-X}^{A+\alpha}$ (SCAN)
-------------------------	------------	--	--------------------------------------	--	--------------------------------------	---	---------------------------------------

When CCE predicts a similar value for all three functionals with a large deviation with respect to the experimental data, the measured $\Delta_f H^{\circ, T_r, \text{exp}}$ might be inaccurate. The conclusion is further confirmed if the quasi-FERE corrected values predict a similar trend. Based on the analysis, the experimental data of FeAl_2O_4 and NiAl_2O_4 might be too low (*i.e.* too negative) by about 120-140 and 80-110 meV/atom, respectively. SrHfO_3 might be too high by about 60-90 meV/atom.

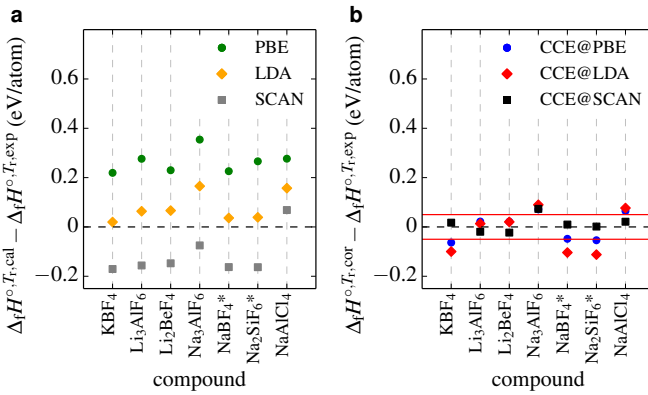


FIG. 4. Uncorrected *vs.* corrected enthalpies for halides. Differences between calculated (a) as well as corrected (b) and experimental room temperature formation enthalpies for seven ternary halides. For the compounds marked with “*” the experimental formation enthalpy from Kubaschewski *et al.* [15] can only be verified by NBS [18]. The red lines at ± 50 meV/atom indicate the typical MAE of previous correction schemes [32, 35].

The scarcity of reliable experimental data for polar ternary systems other than oxides restricts the number of compounds available to demonstrate the generality of CCE. In Figure 4, uncorrected and corrected results are presented for a set of seven ternary halides. The formation enthalpies are listed in Tables A.VIII, A.X, A.XVII and A.XIX with the vibrational, zero-point and thermal contributions in Tables A.XIII and A.XV (Appendix F). Corrections are given in Tables III, A.VIII and A.XVII. It is difficult to ascribe a statistical significance to a set of only seven entries: MAEs amount to 264, 78 and 135, as well as 49, 74 and 24 meV/atom for the uncorrected and corrected results of PBE, LDA and SCAN, respectively. CCE guarantees a significant improvement in all cases. For Na_3AlF_6 , and potentially also NaAlCl_4 , the experimental value might be too low by about 70-90 and 20-80 meV/atom. The accuracy of the corrected results for KBF_4 , NaBF_4 and Na_2SiF_6 is interesting — in these cases part of the corrections are obtained from the gaseous molecular BF_3 and SiF_4 phases and applied to solid ternaries. For PBE and LDA, the corrected results show rather large errors revealing that for these function-

als the corrections per bond are not well transferable from molecules to solids. This biases the MAE particularly for the corrected LDA values. For SCAN, however, the corrected results are accurate, further showcasing the better suitability of this functional for CCE. The functionals’ different behaviors agree with previous reports [66, 67].

The vibrational (zero-point + thermal) contribution to the formation enthalpy can be largely included in the corrections without explicit calculation, being mostly element specific. For example, for binary oxides the vibrational term is highest for Al_2O_3 , BeO and SiO_2 (α -quartz), ranging from 16 to 23 meV/atom (depending on the functional). For ternaries, the largest value is found for kyanite Al_2SiO_5 with 19 to 23 meV/atom. MAEs of the corrected formation energies obtained without vibrational contribution in both the binary-fit and ternary-test sets (as in Refs. [34, 32, 35]) are included in brackets in Table I. They deviate no more than 1 meV/atom from the MAEs of the corrected DFT+AGL results. Thus, $\Delta_f E^{0,\text{DFT}}$ corrections can be reliably based on only $\Delta_f H^{\circ, T_r, \text{exp}}$. In addition, the vibrational term usually does not lead to significant differences between two structures at the same composition. This has already been seen with machine learning analysis [68]. Therefore, the following discussion is based on results directly obtained with DFT.

Relative stability. CCE can also correct the relative stability of same stoichiometry structures with different number of nearest neighbor cation-O bonds. Al_2SiO_5 is an example: kyanite is the experimental ground state and andalusite is higher in energy. PBE falsely predicts kyanite to be 19 meV/atom above andalusite (-2.937 *vs.* -2.956 eV/atom). CCE correctly gives kyanite to be lower by 4 meV/atom (-3.343 *vs.* -3.339 eV/atom), in good agreement with the experimental values (-3.361 *vs.* -3.358 eV/atom).

The situation is more evident with polymorphs having large energy differences. Experimentally, MnO and CoO have rocksalt ground states. In Ref. [23], it was reported that PBE and SCAN predict other ground states for both systems with only 4 cation-O bonds, in disagreement with the experimental finding: 6. CCE solves the issue. We take the DFT ground states provided in Ref. [23], relax and primitivize them. PBE/SCAN for MnO and SCAN for CoO find zincblende (space group $\text{F}\bar{4}3\text{m}$ #216; Pearson symbol cF8; AFLOW prototype $\text{AB}_{\text{c}}\text{F8}_{\text{c}}\text{216}_{\text{c}}\text{a}$ [49, 50, 69]). With PBE the final CoO structure is body-centered tetragonal ($\text{I}\bar{4}\text{m}2$ #119; ti4 ; $\text{AB}_{\text{t}}\text{I4}_{\text{t}}\text{119}_{\text{c}}\text{a}$ [49, 50, 70]). For CoO , PBE and SCAN erroneously give the energies of the relaxed geometries to be 164 and 103 meV/atom below rocksalt. CCE solves the dilemma. When corrected, they become 76 and 20 meV/atom above the experimental ground state. For MnO the PBE structure is corrected from being 5 meV/atom more-stable to 246 meV/atom less-stable than the experimental re-

port. The MnO structure given by SCAN is already 44 meV/atom higher than rocksalt. CCE reduces its difference to 11 meV/atom without changing the correct experimental order. CCE succeeds in all examples. Any scheme dealing only with stoichiometry (such as FERE) would not be able to disentangle the relative stability.

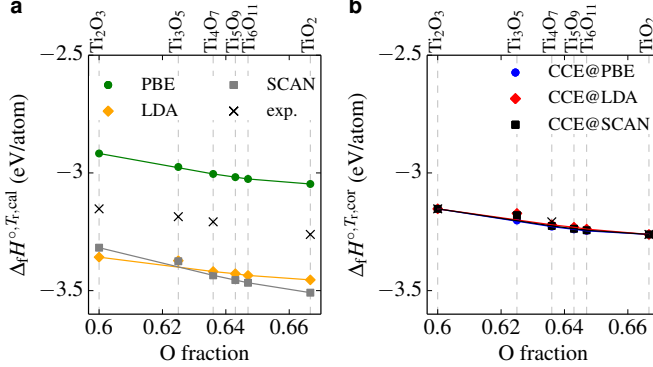


FIG. 5. Uncorrected vs. corrected convex hull. Section of the convex hull between Ti_2O_3 and TiO_2 (rutile) for the Ti-O system from plain DFT (a) and corrected by CCE (b).

Application to Ti-O systems. To test whether CCE will also yield quantitatively reliable results for defect energies, the method is applied to Ti-O. The corrections are obtained from Ti_2O_3 and rutile TiO_2 , and are then applied to predict the enthalpies of other oxides, including crystallographic shear compounds (Magnéli phases) $\text{Ti}_n\text{O}_{2n-1}$. In Figure 5, the section of the convex hull phase diagram [71] between Ti_2O_3 and TiO_2 is presented for both uncorrected and CCE corrected results. Plain DFT captures well the position of all structures with respect to the individual convex hull for each functional, but yields quantitative errors of the order of several 100 meV/atom in all three cases. When corrected by CCE, all three functionals produce formation enthalpies within 10-20 meV/atom of experiments. Note that for all functionals (corrected and uncorrected) and from the experimental data, Ti_3O_5 is found to be above the stability hull by up to about 30 meV/atom.

IV. CONCLUSIONS

We have introduced a Coordination Corrected Enthalpies (CCE) scheme based on the number of nearest neighbor cation-anion bonds. 71 (7) ternary oxides (halides) are used as a test set. CCE gives very accurate corrected formation enthalpies with MAEs of 38 (49), 29 (74) and 27 (24) meV/atom for PBE, LDA and SCAN, respectively. Zero-point and finite temperature vibrational contributions are treated within a quasiharmonic Debye model and are found to largely cancel out. Errors are significantly smaller than previous approaches [32, 34, 35]. Because CCE considers bonding connectivity and topology, it can

also correct the relative stability of different structures at a given composition.

Correction schemes for formation enthalpies are the steps in a ladder of approximations:

- i. The oxygen correction of Ref. [29] applies a constant energy shift per O_2 ; it can be seen as a 0th order step: one parameter for all oxides. The approach typically leads to mean absolute errors of 100 meV/atom or larger, and can be combined with the GGA/GGA+ U mixing scheme for improved accuracy [32].
- ii. The FERE method [34, 35] corrects the elemental reference energy of each species of the compound; it is a 1st order approximation: one parameter per element. FERE's accuracy is typically limited to about 40-50 meV/atom. Improvements require considering the characteristics of the compounds.
- iii. CCE leverages the topology of nearest neighbor shells. CCE yields accurate formation enthalpies with an average absolute error as small as 20-30 meV/atom. The method is simple and easy to extend to other materials classes, *e.g.* nitrides, phosphides or sulfides. It can be used to predict a wide variety of properties relying on accurate formation enthalpies such as battery voltages, defect energies and the formation of high-entropy materials [72].

V. DATA AVAILABILITY.

All the *ab-initio* data are freely available to the public as part of the AFLOW online repository and can be accessed through AFLOW.org following the REST-API interface [45] and AFLUX search language [10].

VI. ACKNOWLEDGMENTS

We thank Ohad Levy, Frisco Rose, Eric Gossett, David Hicks and Denise Ford for fruitful discussions. The authors acknowledge support by DOD-ONR (N00014-15-1-2863, N00014-15-1-2266, N00014-17-1-2090, N00014-16-1-2326, N00014-17-1-2876). R.F. acknowledges support from the Alexander von Humboldt foundation under the Feodor Lynen research fellowship. C.O. acknowledges support from the National Science Foundation Graduate Research Fellowship under Grant No. DGF-1106401. S.C. acknowledges financial support from the Alexander von Humboldt foundation.

VII. AUTHOR CONTRIBUTIONS

R.F. and S.C. proposed the formation enthalpy correction. All authors — R.F., D.U., C.O., A.S., M.F., M.B.N., C.T., S.C. — discussed the results and contributed to the writing of the article.

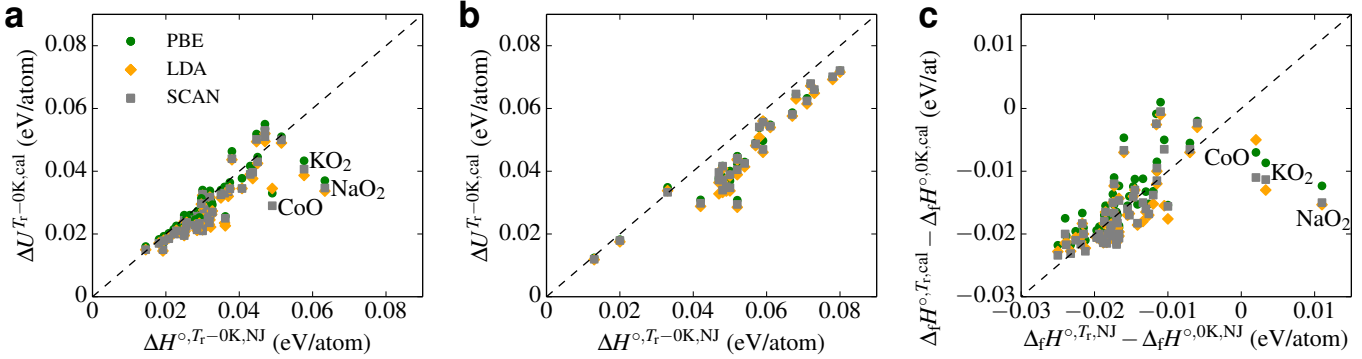


FIG. A.6. **Internal energy *vs.* enthalpy differences.** Calculated internal energy differences *vs.* experimental enthalpy differences from the NIST-JANAF (NJ) collection [16] between 0 and $T_r=298.15$ K for (a) binary and ternary oxides and (b) elemental reference phases. A comparison of the calculated *vs.* experimental formation enthalpy differences for the same set of compounds as in (a) is presented in (c). Points showing significant deviations are labeled with the compound in (a,c).

Appendix A: Comparing experimental enthalpy differences with calculated energy differences

In Figure A.6(a) the calculated internal energy differences from AGL are plotted *vs.* the experimental enthalpy differences [16] between 0 K and T_r for 52 (36 binary and 16 ternary) oxides. The calculated values approximate the measured data in general very well, with a slight tendency to underestimate them. The MAE is 4, 5 and 5 meV/atom for calculations using PBE, LDA and SCAN, respectively. There are three cases with major deviations: NaO₂, KO₂ and CoO. The largest difference between calculated and experimental values occurs for NaO₂: 30 meV/atom for LDA. Superoxides might be difficult to describe within the AGL Debye model. For CoO the deviation of 15–20 meV/atom can be assigned to the general difficulty of describing the properties of the material as noted before for the calculated formation enthalpy in Fig. 2, also recognized previously [35].

In Figure A.6(b) an equivalent plot is presented for 29 mostly metallic elements. The MAE is 8, 10 and 9 meV/atom for PBE, LDA and SCAN. In general, the calculations slightly underestimate the experimental enthalpy difference. This can be understood as the AGL approach neglects electronic contributions to the internal energy change. The errors are significantly smaller than the MAEs of CCE in Fig. 3, which are of the order of 30 meV/atom.

The combined effect of the thermal excitations for the compounds and elements on the formation enthalpy is illustrated in Fig. A.6(c). It depicts the difference ($\Delta_f H^{\circ,T_r,cal} - \Delta_f H^{\circ,0K,cal}$) *vs.* ($\Delta_f H^{\circ,T_r,NJ} - \Delta_f H^{\circ,0K,NJ}$) for the same set of compounds as in Fig. A.6(a). The MAEs are 3, 4 and 4 meV/atom for PBE, LDA and SCAN, indicating that the underestimation of individual enthalpy differences in Figs. A.6(a,b) is partially canceled in the formation enthalpy. The three systems showing large deviations (up to 26 meV/atom for NaO₂) are the same as in Fig. A.6(a): the only compounds with a positive experimental difference between 0 K and T_r . In conclusion,

the AGL approach treats thermal contributions reliably at low computational cost.

Appendix B: Comparing experimental formation enthalpies from different sources

Comparing the data from different experimental sources gives insight on the exact formation enthalpy. Figure A.7 shows the difference between the four collections [15–18] for binary (Figs. A.7(a,b)) and ternary (Figs. A.7(c,d)) oxides. Table A.IV includes the mean absolute deviations. Not all oxides are available in all collections. The number of compounds reported is therefore added in brackets after the name of the collection.

TABLE A.IV. **Comparison of experimental values.** Mean absolute deviations for the experimental formation enthalpies from different sources for binary (above the diagonal) and ternary (below the diagonal) oxides: Kub (Kubaschewski) [15], NJ [16], Barin [17] and NBS [18]. The numbers in brackets after the abbreviations, in the first row for binary and in the first column for ternary oxides, denote the number of oxides for which formation enthalpies were available. The numbers in brackets in the second column are the mean absolute deviation when MgTi₂O₅ is excluded from the set. All values in meV/atom.

	Kub (79)	NJ (41)	Barin (79)	NBS (76)
Kub (71)	-	4	8	14
NJ (16)	20 (7)	-	1	8
Barin (71)	17 (14)	3	-	10
NBS (59)	19 (15)	8	8	-

In general, most of the values for one oxide agree well. However, in certain cases, deviations significantly exceeding ± 50 meV/atom are observed, for which the respective compound is labeled. For the binary oxides in Figs. A.7(a,b), significant deviations always occur when data from the NBS tables are compared to another source as also indicated by the mean absolute deviations in Ta-

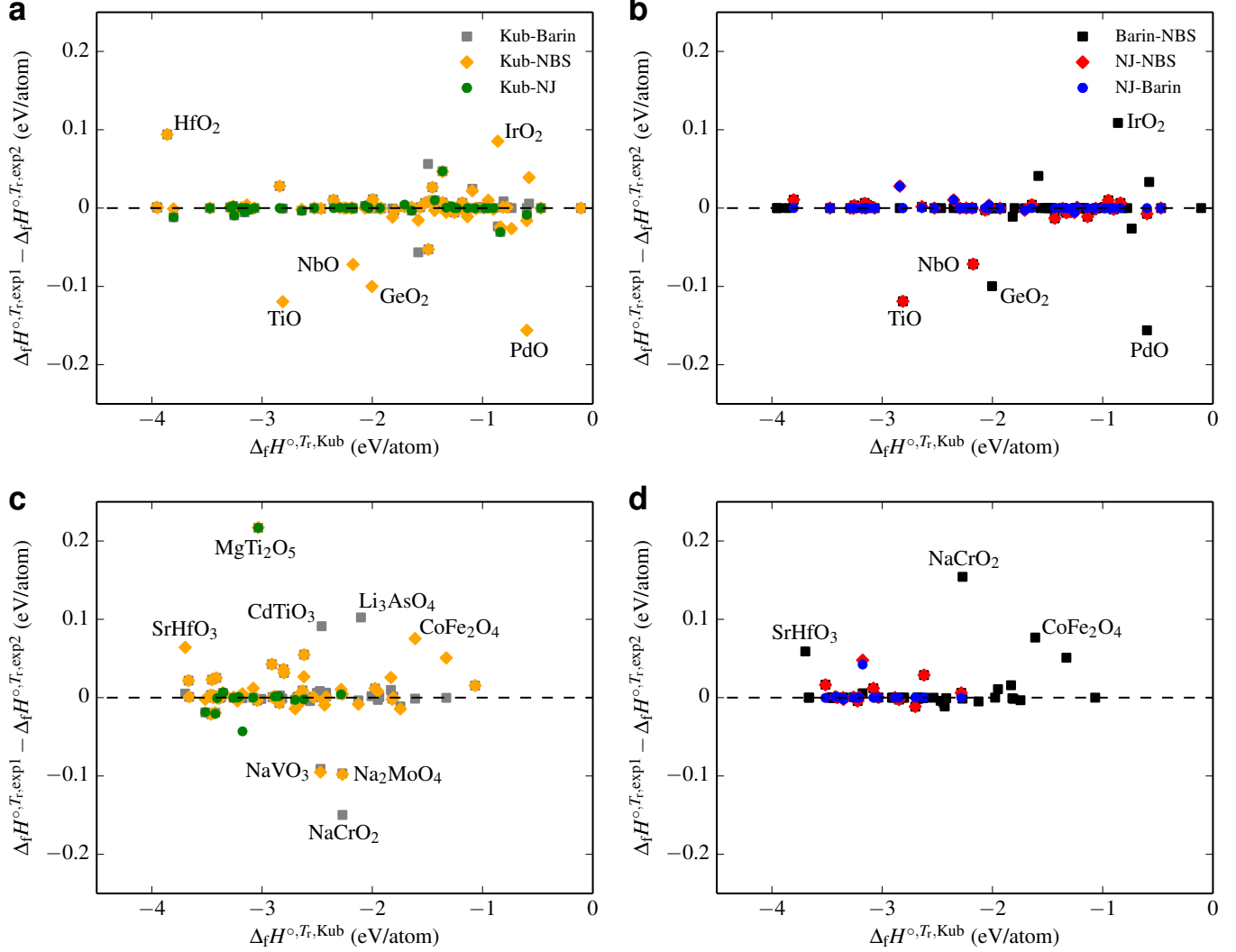


FIG. A.7. Comparison of experimental values. Comparison of the experimental room temperature formation enthalpies from different sources for binary (**a,b**) as well as ternary (**c,d**) oxides. Points showing deviations $\gg \pm 50$ meV/atom are labeled with the compound. Kub refers to Ref. [15], NJ to Ref. [16], Barin to Ref. [17] and NBS to Ref. [18]. Despite corrections can be done to bring MAE to 20-50 meV/atom, there is substantial scatter in experimental measurements.

ble A.IV. The largest values of 14, 10 and 8 meV/atom are found between NBS and the other collections. This might be due to the special internal consistency requirements inside the NBS tables [18].

For ternary oxides significant deviations are seen between Kubaschewski *et al.* and Barin as well as between Kubaschewski *et al.* and NBS in Fig. A.7(c). Some of the formation enthalpies for ternary oxides might not be very accurate in Kubaschewski. For MgTi₂O₅, Kubaschewski $\Delta_f H^{\circ, T_r, \text{exp}}$ is clearly inaccurate since all three other collections suggest the same value, which deviates by more than 200 meV/atom. It is a bias to the mean absolute deviation, especially when compared to NIST-JANAF (NJ) as there are only 16 common ternary oxides within the two collections. Therefore, in the second column in Table A.IV the numbers in brackets were calculated with MgTi₂O₅ excluded. The largest mean absolute deviations

are observed when NBS is involved with the exception of the comparison between Barin and Kubaschewski. In Figure A.7(d) three significant deviations are also found between the Barin and NBS collections. Therefore, the NBS data might not be suited for comparisons with calculated results.

Appendix C: Comparison of the zero-point and thermal contributions to the formation enthalpy

Figures A.8(a,b) depict the individual zero-point and thermal contributions to the formation enthalpy according to Eq. (4) for binary and ternary oxides, respectively. The ZPC is usually larger. Both contributions are typically about two orders of magnitude smaller than the total values of the formation enthalpies. The maximum ab-

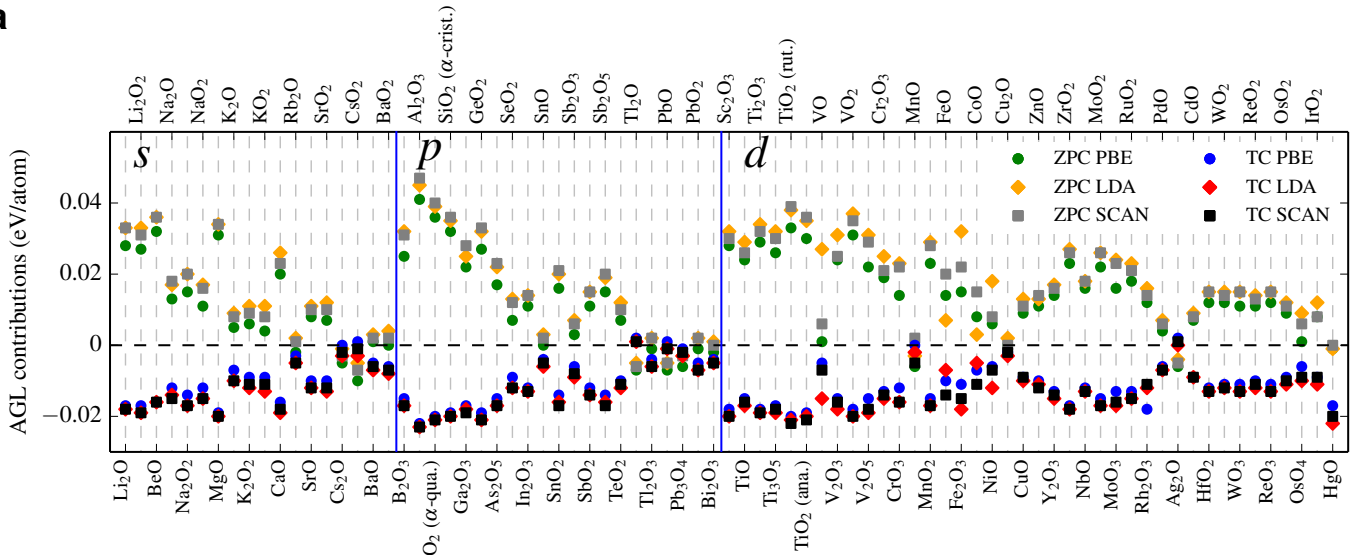
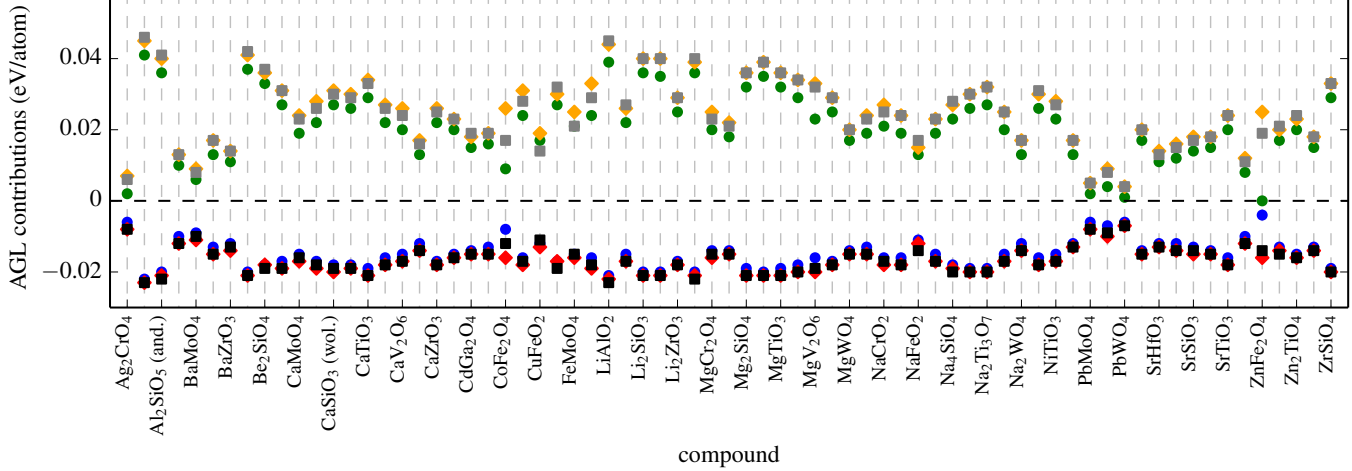
a**b**

FIG. A.8. Zero-point vs. thermal contribution. Comparison of the zero-point (ZPC) and thermal (TC) contributions to the room temperature formation enthalpies for binary (a) and ternary (b) oxides.

solute values of the zero-point contribution (thermal contribution) of 47 (23) and 46 (23) meV/atom are reached for Al₂O₃ and kyanite Al₂SiO₅ for binary and ternary oxides with SCAN, respectively. For binaries, the zero-point contribution is almost always positive (or minimally -10 meV/atom for CsO₂ for PBE), while the thermal is basically always negative (or maximally 2 meV/atom for Ag₂O and Tl₂O for PBE). For ternaries the contributions always have opposite sign leading to a partial cancellation, involving two effects: **i.** the bonds for the ionic compound (for especially light elements) are rather stiff, leading to a large zero-point vibrational energy with respect to the references, giving a positive contribution to the formation enthalpy; **ii.** for systems with stiff bonds, only a small

part of the vibrational spectrum is accessible to thermal excitations, giving a negative contribution to the formation enthalpies, as the enthalpies of the elements increase more strongly with temperature than the compounds.

Appendix D: Dependence of the oxygen correction on the fitting set

According to Wang *et al.* [29], DFT formation energies of oxides can be corrected by plotting the difference between calculated and experimental values for non-transition metal compounds, normalized to O₂ in the formula unit (Fig. A.9). Here, the calculated room tem-

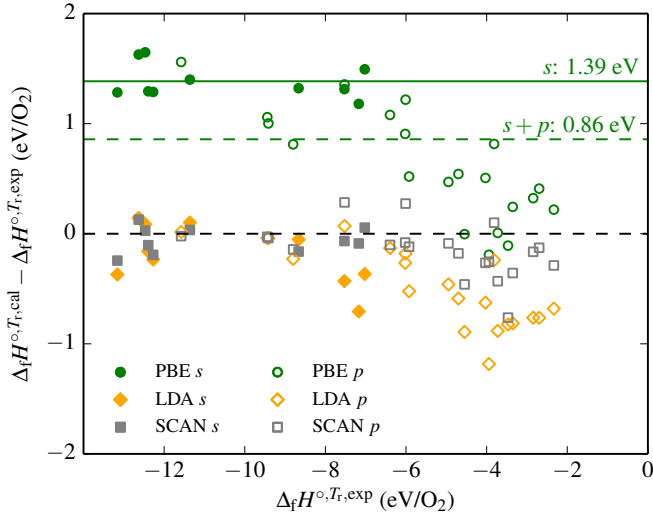


FIG. A.9. Variation of the oxygen correction. Dependence of the oxygen correction on the set of compounds used for the fitting. The filled (open) symbols correspond to *s*-oxides (*p*-oxides). For PBE, the fitting curves are drawn with only the *s*-oxides used to obtain the correction (solid green line) and all *s*- and *p*-oxides are used (dashed green line). The scale is normalized to eV/O₂.

perature formation enthalpies are used. In contrast, the original work considered formation energies directly calculated with DFT. The differences are negligible given the small size of the vibrational contribution. As proposed by Wang *et al.*, [29] the $\Delta_f H^{\circ,T_r,\text{cal}}$ should have a rather constant shift from $\Delta_f H^{\circ,T_r,\text{exp}}$, which was estimated to be 1.36 eV/O₂ for PBE, based on a fit of six non-transition metal (*s*- and *p*-) oxides. The calculated formation enthalpies could then be corrected by subtracting the value.

This is a good approximation for binary *s*-oxides (O²⁻ anions) and PBE (filled green symbols in Fig. A.9): the oxygen correction fitted to the data amounts to 1.39 eV/O₂, in close agreement with the initially proposed value. However, when all *p*-oxides are included (open green symbols in Fig. A.9), a constant shift is not adequate, leading to a very different correction of 0.86 eV. Also, for LDA and SCAN, when the formation enthalpies of *p*-oxides are included, the scatter increases towards lower values. The trend is less pronounced than for PBE.

When fitting the oxygen correction to the formation enthalpies of the *s*-oxides calculated for SCAN, a small value 0.06 eV is obtained. The SCAN binding energy for O₂ (-5.59 eV) is also closer to experiment (-5.12 eV) [16] than PBE (-6.05 eV) and LDA (-7.49 eV), in good agreement with previous reports [22, 29, 34, 62, 73]. As such, the better description of oxides by SCAN *vs.* PBE is mostly due to its improved treatment of O₂.

Appendix E: Importance of *ab-initio* data for CCE

To investigate the importance of the information included in the *ab-initio* data on the accuracy of CCE, we derive the corrections per bond from the experimental binaries and apply to the ternaries without using DFT data (CCE@exp). In Figure A.10, the results are compared to the CCE corrected SCAN data (CCE@SCAN) for the test set of 71 ternary oxides. The MAE is about an order of magnitude higher, *i.e.* 244 *vs.* 27 meV/atom, when using no *ab-initio* data as input, indicating that the information obtained from DFT is essential for CCE: predicting the stability of a compound only from nearest neighbor interactions (CCE@exp) is not a very good approximation. However, the DFT error for the formation enthalpy appears to be rather well reproduced from only nearest neighbor contributions.

Appendix F: Tables with numerical data

TABLE A.V: Structural data. ICSD numbers, space group numbers and Pearson symbols for the structures of 79 binary and 71 ternary oxides. Space-groups and Pearson symbols are calculated with AFLOW-SYM [55].

formula	ICSD #	space group #	Pearson symbol	formula	ICSD #	space group #	Pearson symbol
Li ₂ O	642216	225	cF12	Ag ₂ CrO ₄	16298	62	oP28
Li ₂ O ₂	152183	194	hP8	Al ₂ SiO ₅ (kya.)	85742	2	aP32
BeO	62736	186	hP4	Al ₂ SiO ₅ (and.)	30679	58	oP32
Na ₂ O	60435	225	cF12	BaAl ₂ O ₄	246027	173	hP56
Na ₂ O ₂	25526	189	hP12	BaMoO ₄	50821	88	tI24
NaO ₂	87178	205	cP12	BaTiO ₃	187292	221	cP5
MgO	159378	225	cF8	BaZrO ₃	27048	221	cP5
K ₂ O	180571	225	cF12	BeAl ₂ O ₄	34806	62	oP28
K ₂ O ₂	180559	64	oS16	Be ₂ SiO ₄	64945	148	hR42
KO ₂	38245	139	tI6	CaAl ₄ O ₇	14270	15	mS48
CaO	60704	225	cF8	CaMoO ₄	417513	88	tI24
Rb ₂ O	77906	225	cF12	Ca ₃ SiO ₅	81100	8	mS54
SrO	181061	225	cF8	CaSiO ₃ (wol.)	201537	2	aP30
SrO ₂	647474	139	tI6	CaSiO ₃ (ps-wol.)	87694	15	mS60
Cs ₂ O	27919	166	hR3	CaTiO ₃	165801	62	oP20
CsO ₂	38247	139	tI6	Ca ₂ V ₂ O ₇	421266	2	aP22
BaO	26961	225	cF8	CaV ₂ O ₆	166516	12	mS18

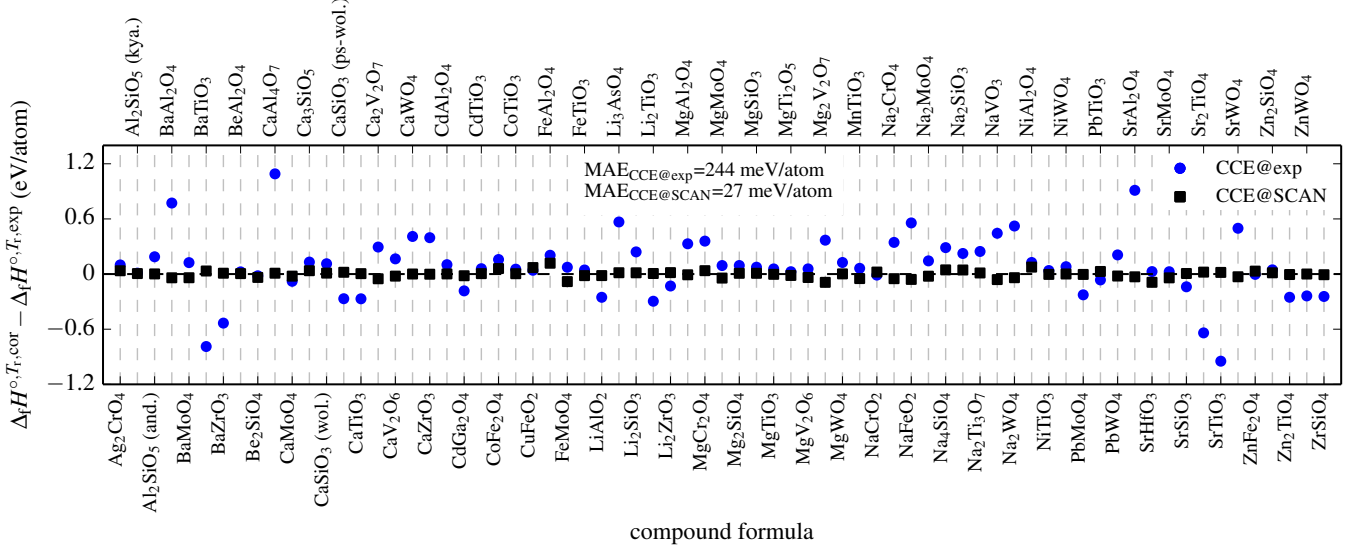


FIG. A.10. **Importance of input data for CCE.** Differences between corrected and experimental room temperature formation enthalpies for the test set of 71 ternary oxides if the CCE method is based on only experimental data for binary oxides (CCE@exp), or applied on top of calculated SCAN results (CCE@SCAN).

TABLE A.V. (continued)

formula	ICSD #	space group #	Pearson symbol	formula	ICSD #	space group #	Pearson symbol
BaO ₂	24248	139	tI6	CaWO ₄	60547	88	tI24
B ₂ O ₃	24649	144	hP15	CaZrO ₃	97463	62	oP20
Al ₂ O ₃	89664	167	hR10	CdAl ₂ O ₄	183382	227	cF56
SiO ₂ (α -qua.)	79635	152	hp9	CdGa ₂ O ₄	159739	227	cF56
SiO ₂ (α -crist.)	153886	92	tP12	CdTiO ₃	15989	148	hR10
Ga ₂ O ₃	83645	12	mS20	CoFe ₂ O ₄	166200	227	cF56
GeO ₂	158597	136	tP6	CoTiO ₃	48107	148	hR10
As ₂ O ₅	654040	19	oP28	CuFeO ₂	246912	166	hR4
SeO ₂	59712	135	tP24	FeAl ₂ O ₄	56117	227	cF56
In ₂ O ₃	33649	206	cI80	FeMoO ₄	43012	12	mS48
SnO	16481	129	tP4	FeTiO ₃	187688	148	hR10
SnO ₂	184420	136	tP6	LiAlO ₂	28288	166	hR4
Sb ₂ O ₃	31102	227	cF80	Li ₃ AsO ₄	75927	31	oP16
SbO ₂	4109	33	oP24	Li ₂ SiO ₃	28192	36	oS24
Sb ₂ O ₅	1422	15	mS28	Li ₂ TiO ₃	162215	15	mS48
TeO ₂	161691	92	tP12	Li ₂ ZrO ₃	94893	15	mS24
Tl ₂ O	16220	166	hR6	MgAl ₂ O ₄	24766	227	cF56
Tl ₂ O ₃	26813	206	cI80	MgCr ₂ O ₄	160953	227	cF56
PbO	53927	129	tP4	MgMoO ₄	20418	12	mS48
Pb ₃ O ₄	29094	135	tP28	Mg ₂ SiO ₄	83793	62	oP28
PbO ₂	34234	136	tP6	MgSiO ₃	30895	14	mP40
Bi ₂ O ₃	168806	14	mP20	MgTiO ₃	171792	148	hR10
Sc ₂ O ₃	647398	206	cI80	MgTi ₂ O ₅	37232	63	oS32
TiO	56694	12	mS20	MgV ₂ O ₆	10391	12	mS18
Ti ₂ O ₃	647550	167	hR10	Mg ₂ V ₂ O ₇	2321	2	aP22
Ti ₃ O ₅	75193	12	mS32	MgWO ₄	67903	13	mP12
TiO ₂ (rut.)	33837	136	tP6	MnTiO ₃	171579	148	hR10
TiO ₂ (ana.)	154602	141	tI12	NaCrO ₂	182235	166	hR4
VO	647627	225	cF8	Na ₂ CrO ₄	76001	63	oS28
V ₂ O ₃	94768	167	hR10	NaFeO ₂	186309	33	oP16
VO ₂	647610	14	mP12	Na ₂ MoO ₄	151970	227	cF56
V ₂ O ₅	60767	59	oP14	Na ₄ SiO ₄	15500	2	aP18
Cr ₂ O ₃	167268	167	hR10	Na ₂ SiO ₃	24664	36	oS24
CrO ₃	16031	40	oS16	Na ₂ Ti ₃ O ₇	15463	11	mP24
MnO	53928	225	cF8	NaVO ₃	2103	15	mS40

TABLE A.V. (*continued*)

formula	ICSD #	space group #	Pearson symbol	formula	ICSD #	space group #	Pearson symbol
MnO ₂	20229	136	tP6	Na ₂ WO ₄	44524	227	cF56
FeO	31081	225	cF8	NiAl ₂ O ₄	608815	227	cF56
Fe ₂ O ₃	201097	167	hR10	NiTiO ₃	33855	148	hR10
CoO	9865	225	cF8	NiWO ₄	16685	13	mP12
NiO	166115	225	cF8	PbMoO ₄	89034	88	tI24
Cu ₂ O	628619	224	cP6	PbTiO ₃	162046	99	tP5
CuO	92368	15	mS8	PbWO ₄	93374	88	tI24
ZnO	163380	186	hP4	SrAl ₂ O ₄	160297	4	mP28
Y ₂ O ₃	27772	206	cI80	SrHfO ₃	84280	62	oP20
ZrO ₂	80043	14	mP12	SrMoO ₄	23700	88	tI24
NbO	27574	221	cP6	SrSiO ₃	32542	5	mS60
MoO ₂	644064	14	mP12	Sr ₂ TiO ₄	157402	139	tI14
MoO ₃	151751	62	oP16	SrTiO ₃	187296	221	cP5
RuO ₂	647377	136	tP6	SrWO ₄	23701	88	tI24
Rh ₂ O ₃	181829	167	hR10	ZnFe ₂ O ₄	91935	227	cF56
PdO	26598	131	tP4	Zn ₂ SiO ₄	20093	148	hR42
Ag ₂ O	174091	224	cP6	Zn ₂ TiO ₄	109093	91	tP28
CdO	181294	225	cF8	ZnWO ₄	156482	13	mP12
HfO ₂	173158	14	mP12	ZrSiO ₄	71942	141	tI24
WO ₂	8217	14	mP12				
WO ₃	84848	14	mP16				
ReO ₂	647349	14	mP12				
ReO ₃	16810	221	cP4				
OsO ₂	647244	136	tP6				
OsO ₄	23803	15	mS20				
IrO ₂	640887	136	tP6				
HgO	14124	62	oP8				

TABLE A.VI: Structural data for halides. ICSD numbers, space group numbers and Pearson symbols for the structures of 9 binary and 7 ternary halides. Space-groups and Pearson symbols are calculated with AFLOW-SYM [55].

formula	ICSD #	space group #	Pearson symbol	formula	ICSD #	space group #	Pearson symbol
LiF	44272	225	cF8	KBF ₄	22260	62	oP24
NaF	52238	225	cF8	Li ₃ AlF ₆	85171	15	mS120
KF	64686	225	cF8	Li ₂ BeF ₄	72423	148	hR42
BeF ₂	261194	152	hP9	Na ₃ AlF ₆	30201	14	mP20
AlF ₃	36034	167	hR8	NaBF ₄	30435	63	oS24
NaCl	162800	225	cF8	Na ₂ SiF ₆	61274	150	hP27
KCl	240527	225	cF8	NaAlCl ₄	71159	19	oP24
CaCl ₂	246416	58	oP6				
AlCl ₃	39566	12	mS16				

TABLE A.VII: Formation enthalpies and CCE corrections for binary oxides. Calculated and experimental room temperature formation enthalpies, corrections per bond $\delta H_{A-O}^{A+\alpha}$, number of cation-oxygen bonds N_{A-O} per formula unit and oxidation states $+\alpha$ of the cation for binary oxides. Experimental values from Kubaschewski *et al.* [15], NIST-JANAF [16] and Barin [17]. Values in brackets denote cases in which the corrections are applied to calculate corrected values (see section III B of the main text for details). The O-O bond correction for peroxides is obtained from Li₂O₂. The O-O bond correction for superoxides is derived from KO₂. The two values are listed in the table at the position of the respective compound. Enthalpies in eV/atom; corrections in eV/bond.

formula	PBE+AGL LDA+AGL SCAN+AGL				Exp.	$\delta H_{A-O}^{A+\alpha}$	$\delta H_{A-O}^{A+\alpha}$	$\delta H_{A-O}^{A+\alpha}$	N_{A-O}	$+\alpha$
	PBE+AGL	LDA+AGL	SCAN+AGL							
Li ₂ O	-1.850	-2.092	-2.083	-2.066	[15]	0.0809	-0.0100	-0.0065	8	+1
Li ₂ O ₂	-1.426	-1.704	-1.605	-1.643	[15]	-0.1050	-0.1270	0.2270	12	+1
BeO	-2.751	-3.122	-3.126	-3.158	[15]	0.2035	0.0180	0.0160	4	+2
Na ₂ O	-1.224	-1.453	-1.471	-1.444	[16]	0.0826	-0.0033	-0.0101	8	+1
Na ₂ O ₂	-1.083	-1.350	-1.285	-1.329	[15]	(-1.304)	(-1.309)	(-1.311)	12	+1
NaO ₂	-0.795	-1.014	-0.893	-0.901	[15]	(-0.777)	(-0.918)	(-0.856)	6	+1
MgO	-2.705	-3.096	-3.111	-3.118	[15]	0.1373	0.0072	0.0023	6	+2
K ₂ O	-1.036	-1.326	-1.266	-1.255	[15]	0.0821	-0.0269	-0.0041	8	+1
K ₂ O ₂	-1.074	-1.387	-1.256	-1.282	[15]	(-1.294)	(-1.275)	(-1.300)	12	+1

TABLE A.VII. (*continued*)

formula	PBE+AGL	LDA+AGL	SCAN+AGL	Exp.	$\delta H_{A-O}^{A+\alpha}$	$\delta H_{A-O}^{A+\alpha}$	$\delta H_{A-O}^{A+\alpha}$	N_{A-O}	$+\alpha$
	PBE+AGL	LDA+AGL	SCAN+AGL						
KO ₂	-0.893	-1.162	-1.014	-0.983 [15]	-0.5500	-0.2680	-0.0520	10	+1
CaO	-2.969	-3.382	-3.351	-3.290 [15]	0.1070	-0.0308	-0.0203	6	+2
Rb ₂ O	-0.922	-1.232	-1.161	-1.171 [15]	0.0934	-0.0229	0.0035	8	+1
SrO	-2.746	-3.127	-3.116	-3.068 [15]	0.1073	-0.0195	-0.0160	6	+2
SrO ₂	-1.902	-2.314	-2.177	-2.189 [15]	(-2.224)	(-2.207)	(-2.199)	10	+2
Cs ₂ O	-0.999	-1.313	-1.210	-1.195 [15]	0.0983	-0.0588	-0.0073	6	+1
CsO ₂	-0.899	-1.175	-1.011	-0.989 [15]	(-1.043)	(-0.890)	(-0.969)	10	+1
BaO	-2.490	-2.815	-2.832	-2.841 [15]	0.1167	0.0085	0.0028	6	+2
BaO ₂	-1.866	-2.255	-2.128	-2.191 [15]	(-2.220)	(-2.241)	(-2.213)	10	+2
B ₂ O ₃	-2.396	-2.708	-2.683	-2.640 [15]	0.2030	-0.0572	-0.0357	6	+3
Al ₂ O ₃	-3.005	-3.469	-3.480	-3.473 [15]	0.1950	0.0020	-0.0028	12	+3
SiO ₂ (α -qua.)	-2.794	-3.160	-3.156	-3.147 [15]	0.2648	-0.0098	-0.0070	4	+4
SiO ₂ (α -crist.)	-2.804	-3.151	-3.151	-3.138 [15]	(-3.157)	(-3.138)	(-3.142)	4	+4
Ga ₂ O ₃	-1.851	-2.237	-2.172	-2.258 [15]	0.2034	0.0105	0.0427	10	+3
GeO ₂	-1.598	-2.064	-1.912	-2.004 [15]	0.2030	-0.0300	0.0457	6	+4
As ₂ O ₅	-1.071	-1.448	-1.326	-1.362 [15]	0.2039	-0.0599	0.0251	10	+5
SeO ₂	-0.705	-1.004	-0.874	-0.778 [15]	0.0730	-0.2267	-0.0960	3	+4
In ₂ O ₃	-1.595	-1.958	-1.950	-1.919 [15]	0.1349	-0.0163	-0.0127	12	+3
SnO	-1.351	-1.611	-1.510	-1.481 [17]	0.0650	-0.0653	-0.0148	4	+2
SnO ₂	-1.704	-2.095	-2.033	-2.007 [17]	0.1512	-0.0442	-0.0133	6	+4
Sb ₂ O ₃	-1.343	-1.622	-1.511	-1.484 [15]	0.1177	-0.1150	-0.0218	6	+3
SbO ₂	-1.386	-1.763	-1.626	-1.567 [15]	(-1.570)	(-1.556)	(-1.556)	5	+3, +5
Sb ₂ O ₅	-1.258	-1.663	-1.533	-1.439 [17]	0.1056	-0.1304	-0.0551	12	+5
TeO ₂	-1.036	-1.389	-1.236	-1.117 [17]	0.0610	-0.2035	-0.0893	4	+4
Tl ₂ O	-0.596	-0.716	-0.705	-0.578 [15]	-0.0090	-0.0687	-0.0635	6	+1
Tl ₂ O ₃	-0.686	-1.038	-0.847	-0.809 [15]	0.0513	-0.0955	-0.0159	12	+3
PbO	-1.138	-1.360	-1.252	-1.137 [15]	-0.0005	-0.1115	-0.0575	4	+2
Pb ₃ O ₄	-1.062	-1.316	-1.187	-1.064 [15]	(-1.108)	(-1.112)	(-1.115)	12	+2, +4
PbO ₂	-0.841	-1.203	-1.003	-0.948 [15]	0.0538	-0.1272	-0.0273	6	+4
Bi ₂ O ₃	-1.240	-1.538	-1.259	-1.183 [15]	-0.0286	-0.1775	-0.0381	10	+3
Sc ₂ O ₃	-3.558	-3.964	-4.006	-3.956 [15]	0.1656	-0.0034	-0.0212	12	+3
TiO	-2.532	-2.961	-2.865	-2.812 [15]	0.1169	-0.0619	-0.0221	4.8	+2
Ti ₂ O ₃	-2.907	-3.344	-3.304	-3.153 [15]	0.1025	-0.0796	-0.0633	12	+3
Ti ₃ O ₅	-2.966	-3.360	-3.364	-3.186 [15]	(-3.205)	(-3.174)	(-3.183)	18	+3, +4
TiO ₂ (rut.)	-3.034	-3.438	-3.491	-3.261 [15]	0.1138	-0.0882	-0.1150	6	+4
TiO ₂ (ana.)	-3.067	-3.449	-3.502	-3.243 [16]	(-3.295)	(-3.273)	(-3.272)	6	+4
VO	-1.450	-1.865	-1.767	-2.237 [15]	0.2623	0.1240	0.1568	6	+2
V ₂ O ₃	-2.282	-2.672	-2.646	-2.526 [15]	0.1018	-0.0608	-0.0498	12	+3
VO ₂	-2.360	-2.749	-2.758	-2.466 [15]	0.0528	-0.1413	-0.1462	6	+4
V ₂ O ₅	-2.301	-2.586	-2.595	-2.295 [15]	-0.0037	-0.2033	-0.2101	10	+5
Cr ₂ O ₃	-1.979	-2.233	-2.390	-2.352 [15]	0.1553	0.0495	-0.0159	12	+3
CrO ₃	-1.651	-1.819	-1.796	-1.521 [15]	-0.1305	-0.2980	-0.2745	4	+6
MnO	-1.247	-1.190	-2.095	-1.994 [15]	0.2492	0.2682	-0.0333	6	+2
MnO ₂	-1.672	-1.977	-2.105	-1.800 [15]	0.0640	-0.0885	-0.1528	6	+4
FeO	-0.877	-1.016	-1.347	-1.410 [16]	0.1775	0.1312	0.0210	6	+2
Fe ₂ O ₃	-1.311	-1.662	-1.857	-1.707 [15]	0.1648	0.0187	-0.0625	12	+3
CoO	-0.512	-0.736	-0.859	-1.232 [15]	0.2398	0.1655	0.1243	6	+2
NiO	-0.475	-0.770	-0.647	-1.242 [15]	0.2555	0.1572	0.1982	6	+2
Cu ₂ O	-0.417	-0.546	-0.507	-0.590 [16]	0.1293	0.0328	0.0618	4	+1
CuO	-0.605	-0.858	-0.793	-0.808 [16]	0.1018	-0.0245	0.0075	4	+2
ZnO	-1.445	-1.730	-1.723	-1.817 [15]	0.1858	0.0433	0.0468	4	+2
Y ₂ O ₃	-3.622	-3.999	-4.063	-3.949 [15]	0.1363	-0.0209	-0.0474	12	+3
ZrO ₂	-3.460	-3.888	-3.931	-3.791 [16]	0.1419	-0.0416	-0.0597	7	+4
NbO	-2.053	-2.422	-2.339	-2.175 [15]	0.0610	-0.1235	-0.0820	4	+2
MoO ₂	-1.966	-2.390	-2.233	-2.031 [15]	0.0327	-0.1797	-0.1008	6	+4
MoO ₃	-1.975	-2.264	-2.180	-1.931 [15]	-0.0440	-0.3335	-0.2490	4	+6
RuO ₂	-1.059	-1.458	-1.271	-1.054 [15]	-0.0027	-0.2020	-0.1085	6	+4
Rh ₂ O ₃	-0.710	-1.060	-0.874	-0.737 [15]	0.0115	-0.1347	-0.0572	12	+3
PdO	-0.485	-0.757	-0.648	-0.599 [15]	0.0568	-0.0793	-0.0250	4	+2
Ag ₂ O	-0.123	-0.183	-0.198	-0.107 [15]	-0.0115	-0.0568	-0.0683	4	+1
CdO	-1.028	-1.292	-1.324	-1.339 [15]	0.1037	0.0158	0.0050	6	+2

TABLE A.VII. (*continued*)

formula	PBE+AGL	LDA+AGL	SCAN+AGL	Exp.	$\delta H_{A-O}^{A+\alpha}$	$\delta H_{A-O}^{A+\alpha}$	$\delta H_{A-O}^{A+\alpha}$	N_{A-O}	$+\alpha$
	PBE+AGL	LDA+AGL	SCAN+AGL						
HfO ₂	-3.577	-4.022	-4.016	-3.955 [17]	0.1617	-0.0290	-0.0263	7	+4
WO ₂	-1.923	-2.352	-2.131	-2.037 [15]	0.0570	-0.1575	-0.0473	6	+4
WO ₃	-2.176	-2.493	-2.385	-2.183 [15]	0.0052	-0.2063	-0.1347	6	+6
ReO ₂	-1.371	-1.797	-1.507	-1.551 [17]	0.0898	-0.1230	0.0218	6	+4
ReO ₃	-1.635	-1.980	-1.764	-1.526 [17]	-0.0722	-0.3027	-0.1582	6	+6
OsO ₂	-0.895	-1.305	-1.015	-1.018 [15]	0.0613	-0.1438	0.0015	6	+4
OsO ₄	-0.999	-1.120	-1.040	-0.816 [15]	-0.2288	-0.3805	-0.2803	4	+8
IrO ₂	-0.799	-1.200	-0.803	-0.838 [17]	0.0198	-0.1808	0.0177	6	+4
HgO	-0.319	-0.557	-0.433	-0.470 [15]	0.1515	-0.0870	0.0375	2	+2

TABLE A.VIII: Formation enthalpies and CCE corrections for binary halides. Calculated and experimental room temperature formation enthalpies, corrections per bond $\delta H_{A-X}^{A+\alpha}$, number of cation-anion bonds N_{A-X} per formula unit and oxidation states $+\alpha$ of the cation for binary halides. Experimental values from Kubaschewski *et al.* [15] and NIST-JANAF [16]. Note that BF₃ and SiF₄ are gaseous molecular systems. Enthalpies in eV/atom; corrections in eV/bond.

formula	PBE+AGL	LDA+AGL	SCAN+AGL	Exp.	$\delta H_{A-X}^{A+\alpha}$	$\delta H_{A-X}^{A+\alpha}$	$\delta H_{A-X}^{A+\alpha}$	N_{A-X}	$+\alpha$
	PBE+AGL	LDA+AGL	SCAN+AGL						
LiF	-2.960	-3.161	-3.342	-3.197 [16]	0.0788	0.0120	-0.0482	6	+1
NaF	-2.732	-2.904	-3.124	-2.982 [16]	0.0833	0.0258	-0.0473	6	+1
KF	-2.731	-2.922	-3.088	-2.946 [16]	0.0718	0.0083	-0.0472	6	+1
BeF ₂	-3.271	-3.472	-3.709	-3.547 [15]	0.2073	0.0563	-0.1215	4	+2
BF ₃ (g)	-2.760	-2.824	-3.067	-2.943 [15]	0.2447	0.1587	-0.1640	3	+3
AlF ₃	-3.540	-3.828	-4.095	-3.913 [15]	0.2488	0.0572	-0.1208	6	+3
SiF ₄ (g)	-3.097	-3.208	-3.470	-3.348 [15]	0.3135	0.1750	-0.1525	4	+4
NaCl	-1.832	-1.961	-2.077	-2.131 [15]	0.1000	0.0568	0.0180	6	+1
KCl	-1.981	-2.116	-2.212	-2.263 [15]	0.0938	0.0488	0.0168	6	+1
CaCl ₂	-2.425	-2.598	-2.701	-2.747 [15]	0.1608	0.0742	0.0227	6	+2
AlCl ₃	-1.538	-1.753	-1.755	-1.828 [15]	0.1933	0.0498	0.0485	6	+3

TABLE A.IX: Uncorrected and CCE corrected formation enthalpies for ternary oxides. Calculated, coordination corrected and experimental room temperature formation enthalpies, number of cation-oxygen bonds $N_{1/2-O}$ per formula unit and oxidation states $+\alpha$ of the cations for ternary oxides. For the cation-oxygen bonds- and oxidation numbers, the first (second) number in the column refers to the first (second) element in the formula. Experimental values from Kubaschewski *et al.* [15], NIST-JANAF [16] and Barin [17]. Enthalpies in eV/atom.

formula	PBE+AGL	LDA+AGL	SCAN+AGL	PBE+AGL	LDA+AGL	SCAN+AGL	Exp.	$N_{1/2-O}$	$+\alpha$
	CCE	CCE	CCE						
Ag ₂ CrO ₄	-1.104	-1.285	-1.302	-1.013	-1.033	-1.047	-1.083 [17]	10, 4	+1, +6
Al ₂ SiO ₅ (kya.)	-2.917	-3.365	-3.363	-3.342	-3.364	-3.356	-3.361 [16]	12, 4	+3, +4
Al ₂ SiO ₅ (and.)	-2.940	-3.354	-3.364	-3.340	-3.352	-3.357	-3.358 [16]	11, 4	+3, +4
BaAl ₂ O ₄	-3.065	-3.402	-3.482	-3.413	-3.413	-3.482	-3.441 [15]	7.5, 8	+2, +3
BaMoO ₄	-2.616	-2.872	-2.876	-2.742	-2.661	-2.714	-2.674 [17]	8, 4	+2, +6
BaTiO ₃	-3.090	-3.526	-3.538	-3.506	-3.440	-3.407	-3.441 [17]	12, 6	+2, +4
BaZrO ₃	-3.302	-3.696	-3.744	-3.752	-3.667	-3.679	-3.689 [17]	12, 6	+2, +4
BeAl ₂ O ₄	-2.953	-3.385	-3.398	-3.403	-3.399	-3.402	-3.407 [15]	4, 12	+2, +3
Be ₂ SiO ₄	-2.778	-3.161	-3.157	-3.162	-3.176	-3.171	-3.134 [16]	8, 4	+2, +4
CaAl ₄ O ₇	-3.064	-3.413	-3.480	-3.368	-3.403	-3.468	-3.477 [17]	5, 16	+2, +3
CaMoO ₄	-2.594	-2.915	-2.886	-2.707	-2.652	-2.693	-2.671 [15]	8, 4	+2, +6
Ca ₃ SiO ₅	-3.002	-3.395	-3.380	-3.334	-3.329	-3.336	-3.373 [15]	18, 4	+2, +4
CaSiO ₃ (wol.)	-3.038	-3.412	-3.410	-3.385	-3.366	-3.379	-3.389 [15]	6.3, 4	+2, +4
CaSiO ₃ (ps-wol.)	-3.018	-3.391	-3.393	-3.401	-3.334	-3.355	-3.375 [15]	8, 4	+2, +4
CaTiO ₃	-3.163	-3.591	-3.608	-3.471	-3.436	-3.438	-3.442 [15]	8, 6	+2, +4
Ca ₂ V ₂ O ₇	-2.804	-3.118	-3.152	-2.928	-2.915	-2.956	-2.905 [15]	13, 9	+2, +5
CaV ₂ O ₆	-2.642	-2.918	-2.951	-2.709	-2.671	-2.704	-2.682 [15]	6, 10	+2, +5
CaWO ₄	-2.661	-2.984	-2.958	-2.807	-2.805	-2.841	-2.842 [17]	8, 4	+2, +6
CaZrO ₃	-3.329	-3.727	-3.759	-3.628	-3.640	-3.663	-3.662 [15]	6, 6	+2, +4
CdAl ₂ O ₄	-2.438	-2.834	-2.838	-2.831	-2.846	-2.837	-2.838 [15]	4, 12	+2, +3
CdGa ₂ O ₄	-1.645	-1.999	-1.949	-2.053	-2.026	-2.025	-2.007 [15]	4, 12	+2, +3
CdTiO ₃	-2.289	-2.629	-2.678	-2.550	-2.542	-2.546	-2.551 [17]	6, 6	+2, +4
CoFe ₂ O ₄	-1.143	-1.458	-1.588	-1.562	-1.585	-1.552	-1.612 [15]	4, 12	+2, +3

TABLE A.IX. (*continued*)

formula	PBE+AGL	LDA+AGL	SCAN+AGL	PBE+AGL	LDA+AGL	SCAN+AGL	Exp.	$N_{1/2-O}$	$+ \alpha$
	CCE	CCE	CCE	CCE	CCE	CCE			
CoTiO ₃	-2.089	-2.418	-2.488	-2.514	-2.511	-2.499	-2.503 [15]	6, 6	+2, +4
CuFeO ₂	-0.920	-1.275	-1.321	-1.232	-1.319	-1.258	-1.329 [15]	2, 6	+1, +3
FeAl ₂ O ₄	-2.400	-2.740	-2.829	-2.836	-2.819	-2.836	-2.954 [17]	4, 12	+2, +3
FeMoO ₄	-1.637	-2.036	-2.058	-1.785	-1.945	-1.913	-1.831 [15]	6, 4	+2, +6
FeTiO ₃	-2.231	-2.506	-2.695	-2.580	-2.557	-2.582	-2.565 [15]	6, 6	+2, +4
LiAlO ₂	-2.720	-3.101	-3.111	-3.133	-3.089	-3.096	-3.080 [15]	6, 6	+1, +3
Li ₃ AsO ₄	-1.939	-2.200	-2.188	-2.162	-2.155	-2.191	-2.205 [17]	12, 4	+1, +5
Li ₂ SiO ₃	-2.545	-2.848	-2.847	-2.829	-2.828	-2.834	-2.848 [15]	8, 4	+1, +4
Li ₂ TiO ₃	-2.653	-2.986	-3.006	-2.929	-2.878	-2.878	-2.884 [15]	12, 6	+1, +4
Li ₂ ZrO ₃	-2.759	-3.076	-3.101	-3.063	-3.015	-3.028	-3.044 [15]	12, 6	+1, +4
MgAl ₂ O ₄	-2.976	-3.393	-3.415	-3.388	-3.401	-3.412	-3.404 [16]	4, 12	+2, +3
MgCr ₂ O ₄	-2.225	-2.458	-2.621	-2.569	-2.547	-2.595	-2.632 [15]	4, 12	+2, +3
MgMoO ₄	-2.371	-2.634	-2.626	-2.479	-2.419	-2.463	-2.419 [15]	6, 4	+2, +6
Mg ₂ SiO ₄	-2.825	-3.203	-3.215	-3.212	-3.209	-3.215	-3.223 [15]	12, 4	+2, +4
MgSiO ₃	-2.812	-3.203	-3.204	-3.188	-3.203	-3.202	-3.210 [15]	6, 4	+2, +4
MgTiO ₃	-2.971	-3.357	-3.398	-3.272	-3.260	-3.263	-3.260 [15]	6, 6	+2, +4
MgTi ₂ O ₅	-3.018	-3.389	-3.437	-3.291	-3.262	-3.266	-3.251 [16]	6, 12	+2, +4
MgV ₂ O ₆	-2.479	-2.783	-2.804	-2.567	-2.562	-2.572	-2.534 [15]	6, 10	+2, +5
Mg ₂ V ₂ O ₇	-2.573	-2.866	-2.911	-2.720	-2.726	-2.761	-2.671 [15]	12, 8	+2, +5
MgWO ₄	-2.446	-2.801	-2.751	-2.589	-2.602	-2.619	-2.621 [15]	6, 6	+2, +6
MnTiO ₃	-2.441	-2.639	-3.044	-2.877	-2.855	-2.866	-2.817 [15]	6, 6	+2, +4
NaCrO ₂	-1.900	-2.118	-2.288	-2.257	-2.187	-2.249	-2.271 [15]	6, 6	+1, +3
Na ₂ CrO ₄	-1.976	-2.179	-2.209	-2.019	-2.004	-2.037	-1.987 [17]	10, 4	+1, +6
NaFeO ₂	-1.552	-1.714	-1.940	-1.800	-1.730	-1.867	-1.809 [15]	4, 4	+1, +3
Na ₂ MoO ₄	-2.120	-2.346	-2.358	-2.236	-2.149	-2.198	-2.175 [17]	12, 4	+1, +6
Na ₄ SiO ₄	-2.093	-2.373	-2.397	-2.376	-2.362	-2.374	-2.420 [15]	18, 4	+1, +4
Na ₂ SiO ₃	-2.361	-2.657	-2.677	-2.675	-2.645	-2.656	-2.700 [15]	10, 4	+1, +4
Na ₂ Ti ₃ O ₇	-2.787	-3.116	-3.167	-3.017	-2.989	-2.995	-3.007 [15]	10, 17	+1, +4
NaVO ₃	-2.345	-2.556	-2.619	-2.442	-2.389	-2.439	-2.379 [17]	6, 4	+1, +5
Na ₂ WO ₄	-2.175	-2.397	-2.417	-2.319	-2.273	-2.322	-2.283 [15]	12, 4	+1, +6
NiAl ₂ O ₄	-2.279	-2.641	-2.659	-2.759	-2.735	-2.768	-2.844 [15]	4, 12	+2, +3
NiTiO ₃	-2.070	-2.398	-2.396	-2.513	-2.481	-2.496	-2.492 [15]	6, 6	+2, +4
NiWO ₄	-1.659	-1.980	-1.886	-1.920	-1.931	-1.949	-1.950 [15]	6, 6	+2, +6
PbMoO ₄	-1.893	-2.134	-2.066	-1.863	-1.763	-1.823	-1.819 [15]	8, 4	+2, +6
PbTiO ₃	-2.350	-2.685	-2.655	-2.463	-2.418	-2.448	-2.476 [15]	8, 5	+2, +4
PbWO ₄	-1.948	-2.187	-2.125	-1.951	-1.901	-1.958	-1.937 [15]	8, 4	+2, +6
SrAl ₂ O ₄	-3.074	-3.419	-3.489	-3.389	-3.405	-3.472	-3.442 [17]	6, 8	+2, +3
SrHfO ₃	-3.416	-3.826	-3.844	-3.782	-3.760	-3.787	-3.697 [15]	8, 6	+2, +4
SrMoO ₄	-2.624	-2.918	-2.905	-2.738	-2.670	-2.717	-2.676 [15]	8, 4	+2, +6
SrSiO ₃	-3.039	-3.401	-3.411	-3.422	-3.362	-3.380	-3.386 [15]	8, 4	+2, +4
Sr ₂ TiO ₄	-3.074	-3.492	-3.506	-3.447	-3.366	-3.366	-3.387 [15]	18, 6	+2, +4
SrTiO ₃	-3.164	-3.596	-3.622	-3.558	-3.444	-3.445	-3.463 [15]	12, 6	+2, +4
SrWO ₄	-2.688	-2.981	-2.973	-2.834	-2.818	-2.862	-2.832 [17]	8, 4	+2, +6
ZnFe ₂ O ₄	-1.288	-1.669	-1.783	-1.676	-1.726	-1.703	-1.735 [17]	4, 12	+2, +3
Zn ₂ SiO ₄	-2.054	-2.376	-2.370	-2.417	-2.420	-2.419	-2.433 [15]	8, 4	+2, +4
Zn ₂ TiO ₄	-2.115	-2.457	-2.479	-2.478	-2.444	-2.448	-2.443 [15]	10, 6	+2, +4
ZnWO ₄	-1.937	-2.282	-2.214	-2.128	-2.119	-2.126	-2.126 [15]	6, 6	+2, +6
ZrSiO ₄	-3.146	-3.579	-3.587	-3.511	-3.518	-3.503	-3.496 [16]	8, 4	+4, +4

TABLE A.X: Uncorrected and CCE corrected formation enthalpies for ternary halides. Calculated, coordination corrected and experimental room temperature formation enthalpies, number of cation-anion bonds $N_{1/2-X}$ per formula unit and oxidation states $+ \alpha$ of the cations for ternary halides. For the cation-oxygen bonds- and oxidation numbers, the first (second) number in the column refers to the first (second) element in the formula. Experimental values from Kubaschewski *et al.* [15] and NIST-JANAF [16]. Enthalpies in eV/atom.

formula	PBE+AGL	LDA+AGL	SCAN+AGL	PBE+AGL	LDA+AGL	SCAN+AGL	Exp.	$N_{1/2-X}$	$+ \alpha$
	CCE	CCE	CCE	CCE	CCE	CCE			
KBF ₄	-3.035	-3.235	-3.425	-3.318	-3.354	-3.237	-3.255 [15]	10, 4	+1, +3
Li ₃ AlF ₆	-3.231	-3.443	-3.663	-3.485	-3.494	-3.526	-3.507 [16]	13.3, 6	+1, +3
Li ₂ BeF ₄	-3.135	-3.299	-3.512	-3.344	-3.345	-3.388	-3.365 [15]	8, 4	+1, +2
Na ₃ AlF ₆	-3.079	-3.267	-3.508	-3.361	-3.343	-3.359	-3.433 [15]	16, 6	+1, +3

TABLE A.X. (*continued*)

formula	PBE+AGL	LDA+AGL	SCAN+AGL	PBE+AGL	LDA+AGL	SCAN+AGL	Exp.	$N_{1/2-X}$	+ α
				CCE	CCE	CCE			
NaBF ₄	-2.961	-3.150	-3.349	-3.235	-3.290	-3.177	-3.187 [15]	8, 4	+1, +3
Na ₂ SiF ₆	-3.088	-3.316	-3.518	-3.408	-3.467	-3.353	-3.354 [15]	12, 6	+1, +4
NaAlCl ₄	-1.696	-1.816	-1.904	-1.909	-1.896	-1.952	-1.973 [16]	5, 4	+1, +3

TABLE A.XI: **Uncorrected and quasi-FERE corrected formation enthalpies for ternary oxides.** Calculated, quasi-FERE corrected and experimental room temperature formation enthalpies for ternary oxides. Experimental values from Kubaschewski *et al.* [15], NIST-JANAF [16] and Barin [17]. Enthalpies in eV/atom.

formula	PBE+AGL	LDA+AGL	SCAN+AGL	PBE+AGL	LDA+AGL	SCAN+AGL	Exp.
	quasi-FERE corr.	Exp.					
Ag ₂ CrO ₄	-1.104	-1.285	-1.302	-1.153	-1.167	-1.163	-1.083 [17]
Al ₂ SiO ₅ (kya.)	-2.917	-3.365	-3.363	-3.339	-3.364	-3.355	-3.361 [16]
Al ₂ SiO ₅ (and.)	-2.940	-3.354	-3.364	-3.361	-3.352	-3.355	-3.358 [16]
BaAl ₂ O ₄	-3.065	-3.402	-3.482	-3.534	-3.431	-3.516	-3.441 [15]
BaMoO ₄	-2.616	-2.872	-2.876	-2.757	-2.660	-2.760	-2.674 [17]
BaTiO ₃	-3.090	-3.526	-3.538	-3.381	-3.430	-3.476	-3.441 [17]
BaZrO ₃	-3.302	-3.696	-3.744	-3.689	-3.674	-3.715	-3.689 [17]
BeAl ₂ O ₄	-2.953	-3.385	-3.398	-3.403	-3.399	-3.402	-3.407 [15]
Be ₂ SiO ₄	-2.778	-3.161	-3.157	-3.158	-3.176	-3.170	-3.134 [16]
CaAl ₄ O ₇	-3.064	-3.413	-3.480	-3.507	-3.402	-3.464	-3.477 [17]
CaMoO ₄	-2.594	-2.915	-2.886	-2.684	-2.642	-2.704	-2.671 [15]
Ca ₃ SiO ₅	-3.002	-3.395	-3.380	-3.330	-3.329	-3.336	-3.373 [15]
CaSiO ₃ (wol.)	-3.038	-3.412	-3.410	-3.372	-3.368	-3.379	-3.389 [15]
CaSiO ₃ (ps-wol.)	-3.018	-3.391	-3.393	-3.353	-3.346	-3.362	-3.375 [15]
CaTiO ₃	-3.163	-3.591	-3.608	-3.394	-3.423	-3.467	-3.442 [15]
Ca ₂ V ₂ O ₇	-2.804	-3.118	-3.152	-2.976	-2.928	-2.996	-2.905 [15]
CaV ₂ O ₆	-2.642	-2.918	-2.951	-2.780	-2.706	-2.774	-2.682 [15]
CaWO ₄	-2.661	-2.984	-2.958	-2.781	-2.730	-2.819	-2.842 [17]
CaZrO ₃	-3.329	-3.727	-3.759	-3.656	-3.632	-3.651	-3.662 [15]
CdAl ₂ O ₄	-2.438	-2.834	-2.838	-2.861	-2.851	-2.838	-2.838 [15]
CdGa ₂ O ₄	-1.645	-1.999	-1.949	-2.024	-2.027	-2.015	-2.007 [15]
CdTiO ₃	-2.289	-2.629	-2.678	-2.517	-2.517	-2.567	-2.551 [17]
CoFe ₂ O ₄	-1.143	-1.458	-1.588	-1.629	-1.657	-1.607	-1.612 [15]
CoTiO ₃	-2.089	-2.418	-2.488	-2.480	-2.486	-2.520	-2.503 [15]
CuFeO ₂	-0.920	-1.275	-1.321	-1.244	-1.345	-1.279	-1.329 [15]
FeAl ₂ O ₄	-2.400	-2.740	-2.829	-2.890	-2.807	-2.804	-2.954 [17]
FeMoO ₄	-1.637	-2.036	-2.058	-1.802	-1.867	-1.873	-1.831 [15]
FeTiO ₃	-2.231	-2.506	-2.695	-2.551	-2.463	-2.550	-2.565 [15]
LiAlO ₂	-2.720	-3.101	-3.111	-3.120	-3.115	-3.134	-3.080 [15]
Li ₃ AsO ₄	-1.939	-2.200	-2.188	-2.228	-2.178	-2.245	-2.205 [17]
Li ₂ SiO ₃	-2.545	-2.848	-2.847	-2.860	-2.855	-2.877	-2.848 [15]
Li ₂ TiO ₃	-2.653	-2.986	-3.006	-2.883	-2.891	-2.945	-2.884 [15]
Li ₂ ZrO ₃	-2.759	-3.076	-3.101	-3.069	-3.042	-3.068	-3.044 [15]
MgAl ₂ O ₄	-2.976	-3.393	-3.415	-3.428	-3.403	-3.413	-3.404 [16]
MgCr ₂ O ₄	-2.225	-2.458	-2.621	-2.544	-2.507	-2.568	-2.632 [15]
MgMoO ₄	-2.371	-2.634	-2.626	-2.492	-2.399	-2.467	-2.419 [15]
Mg ₂ SiO ₄	-2.825	-3.203	-3.215	-3.208	-3.209	-3.214	-3.223 [15]
MgSiO ₃	-2.812	-3.203	-3.204	-3.183	-3.203	-3.200	-3.210 [15]
MgTiO ₃	-2.971	-3.357	-3.398	-3.239	-3.234	-3.283	-3.260 [15]
MgTi ₂ O ₅	-3.018	-3.389	-3.437	-3.249	-3.230	-3.292	-3.251 [16]
MgV ₂ O ₆	-2.479	-2.783	-2.804	-2.638	-2.596	-2.642	-2.534 [15]
Mg ₂ V ₂ O ₇	-2.573	-2.866	-2.911	-2.777	-2.718	-2.780	-2.671 [15]
MgWO ₄	-2.446	-2.801	-2.751	-2.597	-2.585	-2.634	-2.621 [15]
MnTiO ₃	-2.441	-2.639	-3.044	-2.753	-2.665	-2.849	-2.817 [15]
NaCrO ₂	-1.900	-2.118	-2.288	-2.197	-2.187	-2.278	-2.271 [15]
Na ₂ CrO ₄	-1.976	-2.179	-2.209	-2.169	-2.131	-2.153	-1.987 [17]
NaFeO ₂	-1.552	-1.714	-1.940	-1.919	-1.796	-1.902	-1.809 [15]
Na ₂ MoO ₄	-2.120	-2.346	-2.358	-2.244	-2.175	-2.264	-2.175 [17]
Na ₄ SiO ₄	-2.093	-2.373	-2.397	-2.422	-2.427	-2.463	-2.420 [15]
Na ₂ SiO ₃	-2.361	-2.657	-2.677	-2.694	-2.694	-2.723	-2.700 [15]
Na ₂ Ti ₃ O ₇	-2.787	-3.116	-3.167	-2.997	-2.974	-3.046	-3.007 [15]

TABLE A.XI. (*continued*)

formula	PBE+AGL	LDA+AGL	SCAN+AGL	PBE+AGL	LDA+AGL	SCAN+AGL	Exp.
	quasi-FERE corr.						
NaVO ₃	-2.345	-2.556	-2.619	-2.502	-2.410	-2.503	-2.379 [17]
Na ₂ WO ₄	-2.175	-2.397	-2.417	-2.324	-2.243	-2.359	-2.283 [15]
NiAl ₂ O ₄	-2.279	-2.641	-2.659	-2.832	-2.779	-2.825	-2.844 [15]
NiTiO ₃	-2.070	-2.398	-2.396	-2.480	-2.455	-2.516	-2.492 [15]
NiWO ₄	-1.659	-1.980	-1.886	-1.928	-1.914	-1.965	-1.950 [15]
PbMoO ₄	-1.893	-2.134	-2.066	-1.895	-1.823	-1.880	-1.819 [15]
PbTiO ₃	-2.350	-2.685	-2.655	-2.475	-2.471	-2.508	-2.476 [15]
PbWO ₄	-1.948	-2.187	-2.125	-1.980	-1.895	-1.981	-1.937 [15]
SrAl ₂ O ₄	-3.074	-3.419	-3.489	-3.531	-3.423	-3.504	-3.442 [17]
SrHfO ₃	-3.416	-3.826	-3.844	-3.814	-3.786	-3.835	-3.697 [15]
SrMoO ₄	-2.624	-2.918	-2.905	-2.751	-2.676	-2.766	-2.676 [15]
SrSiO ₃	-3.039	-3.401	-3.411	-3.416	-3.394	-3.432	-3.386 [15]
Sr ₂ TiO ₄	-3.074	-3.492	-3.506	-3.393	-3.398	-3.462	-3.387 [15]
SrTiO ₃	-3.164	-3.596	-3.622	-3.439	-3.465	-3.532	-3.463 [15]
SrWO ₄	-2.688	-2.981	-2.973	-2.844	-2.758	-2.877	-2.832 [17]
ZnFe ₂ O ₄	-1.288	-1.669	-1.783	-1.675	-1.751	-1.722	-1.735 [17]
Zn ₂ SiO ₄	-2.054	-2.376	-2.370	-2.413	-2.420	-2.418	-2.433 [15]
Zn ₂ TiO ₄	-2.115	-2.457	-2.479	-2.401	-2.413	-2.449	-2.443 [15]
ZnWO ₄	-1.937	-2.282	-2.214	-2.074	-2.087	-2.126	-2.126 [15]
ZrSiO ₄	-3.146	-3.579	-3.587	-3.483	-3.524	-3.512	-3.496 [16]

TABLE A.XII: **AGL contributions to the formation enthalpies for binary oxides.** Total vibrational (TVC), zero-point (ZPC) and thermal (TC) contributions to the calculated formation enthalpies obtained from AGL [36–40] for each functional for binary oxides. The sum of ZPC and TC might not match exactly the total AGL contribution listed due to rounding. All values in eV/atom.

formula	PBE			LDA			SCAN		
	AGL-TVC	AGL-ZPC	AGL-TC	AGL-TVC	AGL-ZPC	AGL-TC	AGL-TVC	AGL-ZPC	AGL-TC
Li ₂ O	0.011	0.028	-0.017	0.014	0.033	-0.018	0.014	0.033	-0.018
Li ₂ O ₂	0.010	0.027	-0.017	0.014	0.033	-0.019	0.013	0.031	-0.019
BeO	0.017	0.032	-0.016	0.019	0.036	-0.016	0.020	0.036	-0.016
Na ₂ O	0.001	0.013	-0.012	0.002	0.017	-0.014	0.003	0.018	-0.015
Na ₂ O ₂	0.001	0.015	-0.014	0.003	0.020	-0.017	0.003	0.020	-0.017
NaO ₂	-0.001	0.011	-0.012	0.002	0.017	-0.015	0.001	0.016	-0.015
MgO	0.012	0.031	-0.019	0.014	0.034	-0.020	0.014	0.034	-0.020
K ₂ O	-0.003	0.005	-0.007	-0.001	0.009	-0.010	-0.002	0.008	-0.010
K ₂ O ₂	-0.003	0.006	-0.009	-0.002	0.011	-0.012	-0.002	0.009	-0.011
KO ₂	-0.005	0.004	-0.009	-0.002	0.011	-0.013	-0.003	0.008	-0.011
CaO	0.004	0.020	-0.016	0.007	0.026	-0.019	0.005	0.023	-0.018
Rb ₂ O	-0.004	-0.002	-0.003	-0.004	0.002	-0.005	-0.004	0.001	-0.005
SrO	-0.002	0.008	-0.010	-0.001	0.011	-0.012	-0.001	0.010	-0.012
SrO ₂	-0.003	0.007	-0.010	-0.001	0.012	-0.013	-0.002	0.010	-0.012
Cs ₂ O	-0.005	-0.005	0	-0.004	-0.001	-0.003	-0.005	-0.003	-0.002
CsO ₂	-0.009	-0.010	0.001	-0.008	-0.005	-0.003	-0.008	-0.007	-0.001
BaO	-0.005	0.001	-0.005	-0.004	0.003	-0.007	-0.004	0.002	-0.006
BaO ₂	-0.006	0	-0.006	-0.004	0.004	-0.008	-0.005	0.002	-0.007
B ₂ O ₃	0.009	0.025	-0.015	0.015	0.032	-0.017	0.014	0.031	-0.017
Al ₂ O ₃	0.019	0.041	-0.022	0.022	0.045	-0.023	0.023	0.047	-0.023
SiO ₂ (α -qua.)	0.016	0.036	-0.020	0.018	0.039	-0.021	0.018	0.040	-0.021
SiO ₂ (α -crist.)	0.013	0.032	-0.019	0.015	0.035	-0.020	0.016	0.036	-0.020
Ga ₂ O ₃	0.005	0.022	-0.017	0.007	0.025	-0.018	0.008	0.028	-0.019
GeO ₂	0.008	0.027	-0.019	0.011	0.032	-0.021	0.012	0.033	-0.021
As ₂ O ₅	0.003	0.017	-0.015	0.005	0.022	-0.017	0.006	0.023	-0.017
SeO ₂	-0.002	0.007	-0.009	0.001	0.013	-0.012	0	0.012	-0.012
In ₂ O ₃	-0.001	0.011	-0.012	0.001	0.014	-0.013	0.001	0.014	-0.013
SnO	-0.004	0	-0.004	-0.003	0.003	-0.006	-0.003	0.002	-0.005
SnO ₂	0.001	0.016	-0.014	0.003	0.020	-0.016	0.004	0.021	-0.017
Sb ₂ O ₃	-0.004	0.003	-0.006	-0.002	0.007	-0.009	-0.002	0.006	-0.008
SbO ₂	-0.001	0.011	-0.012	0.001	0.015	-0.014	0.001	0.015	-0.014
Sb ₂ O ₅	0.001	0.015	-0.014	0.003	0.019	-0.016	0.004	0.020	-0.017
TeO ₂	-0.002	0.007	-0.010	0	0.012	-0.012	-0.001	0.010	-0.011

TABLE A.XII. (*continued*)

formula	PBE			LDA			SCAN		
	AGL-TVC	AGL-ZPC	AGL-TC	AGL-TVC	AGL-ZPC	AGL-TC	AGL-TVC	AGL-ZPC	AGL-TC
Tl ₂ O	-0.005	-0.007	0.002	-0.004	-0.005	0.001	-0.005	-0.006	0.001
Tl ₂ O ₃	-0.006	-0.001	-0.004	-0.005	0.002	-0.006	-0.005	0.002	-0.006
PbO	-0.006	-0.007	0.001	-0.006	-0.005	-0.001	-0.006	-0.005	-0.001
Pb ₃ O ₄	-0.006	-0.006	-0.001	-0.006	-0.003	-0.003	-0.006	-0.003	-0.002
PbO ₂	-0.006	-0.001	-0.005	-0.004	0.002	-0.007	-0.005	0.002	-0.007
Bi ₂ O ₃	-0.006	-0.002	-0.004	-0.005	0.001	-0.005	-0.005	0	-0.005
Sc ₂ O ₃	0.009	0.028	-0.018	0.012	0.032	-0.020	0.011	0.030	-0.020
TiO	0.009	0.024	-0.015	0.012	0.029	-0.017	0.010	0.026	-0.016
Ti ₂ O ₃	0.011	0.029	-0.018	0.014	0.034	-0.019	0.013	0.032	-0.019
Ti ₃ O ₅	0.009	0.026	-0.017	0.013	0.032	-0.019	0.012	0.03	-0.018
TiO ₂ (rut.)	0.013	0.033	-0.020	0.016	0.038	-0.021	0.017	0.039	-0.022
TiO ₂ (ana.)	0.012	0.030	-0.019	0.014	0.035	-0.020	0.015	0.036	-0.021
VO	-0.004	0.001	-0.005	0.011	0.027	-0.015	0	0.006	-0.007
V ₂ O ₃	0.008	0.024	-0.015	0.013	0.031	-0.018	0.009	0.025	-0.016
VO ₂	0.012	0.031	-0.018	0.017	0.037	-0.020	0.015	0.035	-0.020
V ₂ O ₅	0.006	0.022	-0.015	0.012	0.031	-0.019	0.011	0.029	-0.018
Cr ₂ O ₃	0.006	0.019	-0.013	0.010	0.025	-0.015	0.007	0.021	-0.014
CrO ₃	0.002	0.014	-0.012	0.007	0.023	-0.016	0.007	0.022	-0.016
MnO	-0.006	-0.006	0	-0.005	-0.003	-0.002	-0.002	0.002	-0.005
MnO ₂	0.008	0.023	-0.015	0.012	0.029	-0.017	0.011	0.028	-0.017
FeO	0.004	0.014	-0.010	0	0.007	-0.007	0.006	0.020	-0.014
Fe ₂ O ₃	0.004	0.015	-0.011	0.014	0.032	-0.018	0.007	0.022	-0.015
CoO	0.001	0.008	-0.007	-0.002	0.003	-0.005	0.004	0.015	-0.011
NiO	-0.001	0.006	-0.006	0.006	0.018	-0.012	0.001	0.008	-0.007
Cu ₂ O	-0.002	0	-0.002	-0.002	0.002	-0.003	-0.002	0	-0.002
CuO	0.001	0.009	-0.009	0.003	0.013	-0.010	0.002	0.011	-0.009
ZnO	0.001	0.011	-0.010	0.002	0.013	-0.011	0.003	0.014	-0.012
Y ₂ O ₃	0.001	0.014	-0.013	0.003	0.017	-0.015	0.002	0.016	-0.014
ZrO ₂	0.006	0.023	-0.017	0.008	0.027	-0.018	0.008	0.026	-0.018
NbO	0.004	0.016	-0.012	0.005	0.018	-0.013	0.005	0.018	-0.013
MoO ₂	0.007	0.022	-0.015	0.009	0.026	-0.017	0.009	0.026	-0.017
MoO ₃	0.003	0.016	-0.013	0.007	0.024	-0.017	0.007	0.023	-0.016
RuO ₂	0.004	0.018	-0.013	0.007	0.023	-0.015	0.006	0.021	-0.015
Rh ₂ O ₃	-0.006	0.012	-0.018	0.004	0.016	-0.012	0.003	0.014	-0.011
PdO	-0.002	0.004	-0.006	0	0.007	-0.007	-0.001	0.006	-0.007
Ag ₂ O	-0.004	-0.006	0.002	-0.004	-0.004	0	-0.004	-0.005	0.001
CdO	-0.002	0.007	-0.009	-0.001	0.009	-0.009	-0.001	0.008	-0.009
HfO ₂	0	0.012	-0.012	0.001	0.015	-0.013	0.001	0.015	-0.013
WO ₂	0.001	0.012	-0.011	0.002	0.015	-0.012	0.002	0.014	-0.012
WO ₃	0	0.011	-0.011	0.002	0.015	-0.013	0.002	0.015	-0.013
ReO ₂	0	0.011	-0.010	0.002	0.014	-0.012	0.002	0.013	-0.011
ReO ₃	0.001	0.012	-0.011	0.002	0.015	-0.013	0.002	0.015	-0.013
OsO ₂	-0.001	0.009	-0.009	0.001	0.012	-0.011	0.001	0.011	-0.010
OsO ₄	-0.005	0.001	-0.006	-0.001	0.009	-0.010	-0.002	0.006	-0.009
IrO ₂	-0.001	0.008	-0.009	0.001	0.012	-0.011	-0.001	0.008	-0.009
HgO	-0.019	-0.001	-0.017	-0.022	-0.001	-0.022	-0.020	0	-0.020

TABLE A.XIII: **AGL contributions to the formation enthalpies for binary halides.** Total vibrational (TVC), zero-point (ZPC) and thermal (TC) contributions to the calculated formation enthalpies obtained from AGL [36–40] for each functional for binary halides. Note that BF₃ and SiF₄ are gaseous molecular systems. The sum of ZPC and TC might not match exactly the total AGL contribution listed due to rounding. All values in eV/atom.

formula	PBE			LDA			SCAN		
	AGL-TVC	AGL-ZPC	AGL-TC	AGL-TVC	AGL-ZPC	AGL-TC	AGL-TVC	AGL-ZPC	AGL-TC
LiF	0.012	0.023	-0.011	0.015	0.029	-0.014	0.015	0.028	-0.013
NaF	0.008	0.017	-0.009	0.010	0.022	-0.013	0.009	0.022	-0.013
KF	0.005	0.010	-0.005	0.007	0.016	-0.009	0.006	0.014	-0.008
BeF ₂	0.008	0.016	-0.007	0.011	0.021	-0.010	0.011	0.021	-0.009
BF ₃ (g)	0.026	0.034	-0.007	0.026	0.033	-0.007	0.026	0.033	-0.007
AlF ₃	0.020	0.036	-0.015	0.023	0.041	-0.018	0.024	0.042	-0.018
SiF ₄ (g)	0.024	0.036	-0.012	0.024	0.036	-0.012	0.024	0.035	-0.011

TABLE A.XIII. (*continued*)

formula	PBE			LDA			SCAN		
	AGL-TVC	AGL-ZPC	AGL-TC	AGL-TVC	AGL-ZPC	AGL-TC	AGL-TVC	AGL-ZPC	AGL-TC
NaCl	0.008	0.009	-0.001	0.009	0.013	-0.004	0.009	0.011	-0.002
KCl	0.008	0.007	0	0.008	0.011	-0.003	0.008	0.010	-0.002
CaCl ₂	0.011	0.012	0	0.013	0.016	-0.003	0.012	0.014	-0.002
AlCl ₃	0.013	0.014	-0.001	0.015	0.019	-0.004	0.015	0.018	-0.003

TABLE A.XIV: **AGL contributions to the formation enthalpies for ternary oxides.** Total vibrational (TVC), zero-point (ZPC) and thermal (TC) contributions to the calculated formation enthalpies obtained from AGL [36–40] for each functional for ternary oxides. The sum of ZPC and TC might not match exactly the total AGL contribution listed due to rounding. All values in eV/atom.

formula	PBE			LDA			SCAN		
	AGL-TVC	AGL-ZPC	AGL-TC	AGL-TVC	AGL-ZPC	AGL-TC	AGL-TVC	AGL-ZPC	AGL-TC
Ag ₂ CrO ₄	-0.003	0.002	-0.006	-0.001	0.007	-0.008	-0.002	0.006	-0.008
Al ₂ SiO ₅ (kya.)	0.019	0.041	-0.022	0.022	0.045	-0.023	0.023	0.046	-0.023
Al ₂ SiO ₅ (and.)	0.016	0.036	-0.020	0.019	0.040	-0.021	0.019	0.041	-0.022
BaAl ₂ O ₄	0	0.010	-0.010	0.001	0.013	-0.012	0.001	0.013	-0.012
BaMoO ₄	-0.003	0.006	-0.009	-0.001	0.009	-0.011	-0.002	0.008	-0.010
BaTiO ₃	0	0.013	-0.013	0.002	0.017	-0.015	0.002	0.017	-0.015
BaZrO ₃	-0.001	0.011	-0.012	0.001	0.014	-0.014	0	0.014	-0.013
BeAl ₂ O ₄	0.017	0.037	-0.020	0.020	0.041	-0.021	0.021	0.042	-0.021
Be ₂ SiO ₄	0.016	0.033	-0.018	0.018	0.036	-0.018	0.019	0.037	-0.019
CaAl ₄ O ₇	0.010	0.027	-0.017	0.012	0.031	-0.019	0.012	0.031	-0.019
CaMoO ₄	0.004	0.019	-0.015	0.007	0.024	-0.017	0.006	0.023	-0.016
Ca ₃ SiO ₅	0.006	0.022	-0.017	0.008	0.028	-0.019	0.008	0.026	-0.018
CaSiO ₃ (wol.)	0.009	0.027	-0.018	0.011	0.031	-0.020	0.010	0.030	-0.019
CaSiO ₃ (ps-wol.)	0.008	0.026	-0.018	0.011	0.030	-0.019	0.010	0.029	-0.019
CaTiO ₃	0.010	0.029	-0.019	0.013	0.034	-0.021	0.012	0.033	-0.021
Ca ₂ V ₂ O ₇	0.006	0.022	-0.016	0.009	0.027	-0.018	0.008	0.026	-0.018
CaV ₂ O ₆	0.005	0.020	-0.015	0.009	0.026	-0.017	0.007	0.024	-0.017
CaWO ₄	0.001	0.013	-0.012	0.003	0.017	-0.014	0.002	0.016	-0.014
CaZrO ₃	0.005	0.022	-0.017	0.007	0.026	-0.018	0.007	0.025	-0.018
CdAl ₂ O ₄	0.005	0.020	-0.015	0.007	0.023	-0.016	0.007	0.023	-0.016
CdGa ₂ O ₄	0.002	0.015	-0.014	0.003	0.018	-0.015	0.003	0.019	-0.015
CdTiO ₃	0.002	0.016	-0.013	0.004	0.019	-0.015	0.004	0.019	-0.015
CoFe ₂ O ₄	0.001	0.009	-0.008	0.011	0.026	-0.016	0.005	0.017	-0.012
CoTiO ₃	0.008	0.024	-0.016	0.013	0.031	-0.018	0.011	0.028	-0.017
CuFeO ₂	0.005	0.017	-0.012	0.006	0.019	-0.013	0.003	0.014	-0.011
FeAl ₂ O ₄	0.010	0.027	-0.017	0.013	0.030	-0.017	0.014	0.032	-0.019
FeMoO ₄	0.006	0.021	-0.015	0.009	0.025	-0.016	0.006	0.021	-0.015
FeTiO ₃	0.008	0.024	-0.016	0.014	0.033	-0.019	0.012	0.029	-0.018
LiAlO ₂	0.018	0.039	-0.021	0.021	0.044	-0.022	0.022	0.045	-0.023
Li ₃ AsO ₄	0.007	0.022	-0.015	0.009	0.026	-0.017	0.010	0.027	-0.017
Li ₂ SiO ₃	0.016	0.036	-0.020	0.019	0.040	-0.021	0.019	0.040	-0.021
Li ₂ TiO ₃	0.015	0.035	-0.020	0.019	0.040	-0.021	0.019	0.040	-0.021
Li ₂ ZrO ₃	0.009	0.025	-0.017	0.011	0.029	-0.018	0.011	0.029	-0.018
MgAl ₂ O ₄	0.015	0.036	-0.020	0.018	0.039	-0.021	0.018	0.040	-0.022
MgCr ₂ O ₄	0.006	0.020	-0.014	0.009	0.025	-0.016	0.008	0.023	-0.015
MgMoO ₄	0.004	0.018	-0.014	0.007	0.022	-0.015	0.006	0.021	-0.015
Mg ₂ SiO ₄	0.013	0.032	-0.019	0.015	0.036	-0.021	0.015	0.036	-0.021
MgSiO ₃	0.015	0.035	-0.020	0.018	0.039	-0.021	0.018	0.039	-0.021
MgTiO ₃	0.012	0.032	-0.019	0.015	0.036	-0.021	0.015	0.036	-0.021
MgTi ₂ O ₅	0.011	0.029	-0.018	0.014	0.034	-0.020	0.014	0.034	-0.020
MgV ₂ O ₆	0.007	0.023	-0.016	0.014	0.033	-0.020	0.013	0.032	-0.019
Mg ₂ V ₂ O ₇	0.008	0.025	-0.017	0.011	0.029	-0.018	0.011	0.029	-0.018
MgWO ₄	0.003	0.017	-0.014	0.005	0.020	-0.015	0.005	0.020	-0.015
MnTiO ₃	0.005	0.019	-0.013	0.009	0.024	-0.015	0.008	0.023	-0.015
NaCrO ₂	0.005	0.021	-0.016	0.009	0.027	-0.018	0.008	0.025	-0.017
Na ₂ CrO ₄	0.004	0.019	-0.016	0.007	0.024	-0.018	0.007	0.024	-0.018
NaFeO ₂	0.002	0.013	-0.011	0.002	0.015	-0.012	0.003	0.017	-0.014
Na ₂ MoO ₄	0.004	0.019	-0.015	0.006	0.023	-0.017	0.006	0.023	-0.017
Na ₄ SiO ₄	0.006	0.023	-0.018	0.008	0.027	-0.019	0.008	0.028	-0.020

TABLE A.XIV. (*continued*)

formula	PBE			LDA			SCAN		
	AGL-TVC	AGL-ZPC	AGL-TC	AGL-TVC	AGL-ZPC	AGL-TC	AGL-TVC	AGL-ZPC	AGL-TC
Na ₂ SiO ₃	0.008	0.026	-0.019	0.010	0.030	-0.020	0.010	0.030	-0.020
Na ₂ Ti ₃ O ₇	0.009	0.027	-0.019	0.012	0.032	-0.020	0.012	0.032	-0.020
NaVO ₃	0.005	0.020	-0.015	0.008	0.025	-0.017	0.007	0.025	-0.017
Na ₂ WO ₄	0.001	0.013	-0.012	0.003	0.017	-0.014	0.003	0.017	-0.014
NiAl ₂ O ₄	0.010	0.026	-0.016	0.013	0.030	-0.018	0.013	0.031	-0.018
NiTiO ₃	0.008	0.023	-0.015	0.011	0.028	-0.017	0.010	0.027	-0.017
NiWO ₄	0.002	0.013	-0.012	0.004	0.017	-0.013	0.004	0.017	-0.013
PbMoO ₄	-0.004	0.002	-0.006	-0.003	0.005	-0.008	-0.003	0.005	-0.008
PbTiO ₃	-0.003	0.004	-0.007	-0.001	0.009	-0.010	-0.001	0.008	-0.009
PbWO ₄	-0.005	0.001	-0.006	-0.003	0.004	-0.007	-0.004	0.004	-0.007
SrAl ₂ O ₄	0.003	0.017	-0.014	0.005	0.020	-0.015	0.005	0.020	-0.015
SrHfO ₃	-0.001	0.011	-0.012	0	0.014	-0.013	0	0.013	-0.013
SrMoO ₄	0	0.012	-0.012	0.002	0.016	-0.014	0.001	0.015	-0.014
SrSiO ₃	0.001	0.014	-0.013	0.003	0.018	-0.015	0.003	0.017	-0.014
Sr ₂ TiO ₄	0.001	0.015	-0.014	0.003	0.018	-0.015	0.003	0.018	-0.015
SrTiO ₃	0.004	0.020	-0.016	0.006	0.024	-0.018	0.006	0.024	-0.018
SrWO ₄	-0.002	0.008	-0.010	0	0.012	-0.012	0	0.011	-0.012
ZnFe ₂ O ₄	-0.003	0	-0.004	0.009	0.025	-0.016	0.005	0.019	-0.014
Zn ₂ SiO ₄	0.004	0.017	-0.013	0.006	0.020	-0.014	0.006	0.021	-0.015
Zn ₂ TiO ₄	0.005	0.020	-0.015	0.007	0.023	-0.016	0.008	0.024	-0.016
ZnWO ₄	0.002	0.015	-0.013	0.004	0.018	-0.014	0.004	0.018	-0.014
ZrSiO ₄	0.011	0.029	-0.019	0.013	0.033	-0.020	0.013	0.033	-0.020

TABLE A.XV: **AGL contributions to the formation enthalpies for ternary halides.** Total vibrational (TVC), zero-point (ZPC) and thermal (TC) contributions to the calculated formation enthalpies obtained from AGL [36–40] for each functional for ternary halides. The sum of ZPC and TC might not match exactly the total AGL contribution listed due to rounding. All values in eV/atom.

formula	PBE			LDA			SCAN		
	AGL-TVC	AGL-ZPC	AGL-TC	AGL-TVC	AGL-ZPC	AGL-TC	AGL-TVC	AGL-ZPC	AGL-TC
KBF ₄	0.005	0.013	-0.008	0.008	0.020	-0.012	0.007	0.018	-0.011
Li ₃ AlF ₆	0.016	0.029	-0.013	0.019	0.034	-0.016	0.019	0.034	-0.015
Li ₂ BeF ₄	0.009	0.018	-0.008	0.012	0.022	-0.010	0.011	0.022	-0.010
Na ₃ AlF ₆	0.011	0.022	-0.011	0.013	0.026	-0.013	0.013	0.026	-0.013
NaBF ₄	0.008	0.019	-0.010	0.011	0.025	-0.013	0.011	0.024	-0.013
Na ₂ SiF ₆	0.015	0.028	-0.014	0.017	0.033	-0.016	0.017	0.033	-0.016
NaAlCl ₄	0.010	0.009	0.001	0.012	0.015	-0.003	0.012	0.014	-0.002

TABLE A.XVI: **Formation energies and CCE corrections for binary oxides.** DFT formation energies (without vibrational contribution) and experimental room temperature formation enthalpies, corrections per bond $\delta H_{A-O}^{A+\alpha}$, number of cation-oxygen bonds N_{A-O} per formula unit and oxidation states $+\alpha$ of the cation for binary oxides. Experimental values from Kubaschewski *et al.* [15], NIST-JANAF [16] and Barin [17]. Values in brackets denote cases in which the corrections are applied to calculate corrected values (see section III B of the main text for details). The O-O bond correction for peroxides is obtained from Li₂O₂. The O-O bond correction for superoxides is derived from KO₂. The two values are listed in the table at the position of the respective compound. Energies and enthalpies in eV/atom; corrections in eV/bond.

formula	PBE	LDA	SCAN	Exp.	$\delta H_{A-O}^{A+\alpha}$ PBE	$\delta H_{A-O}^{A+\alpha}$ LDA	$\delta H_{A-O}^{A+\alpha}$ SCAN	N_{A-O}	$+\alpha$
Li ₂ O	-1.861	-2.107	-2.097	-2.066 [15]	0.0766	-0.0154	-0.0118	8	+1
Li ₂ O ₂	-1.436	-1.718	-1.618	-1.643 [15]	-0.0930	-0.1160	0.2400	12	+1
BeO	-2.768	-3.142	-3.146	-3.158 [15]	0.1953	0.0083	0.0060	4	+2
Na ₂ O	-1.225	-1.455	-1.474	-1.444 [16]	0.0823	-0.0043	-0.0113	8	+1
Na ₂ O ₂	-1.084	-1.354	-1.288	-1.329 [15]	(-1.307)	(-1.312)	(-1.314)	12	+1
NaO ₂	-0.794	-1.016	-0.894	-0.901 [15]	(-0.776)	(-0.918)	(-0.855)	6	+1
MgO	-2.717	-3.110	-3.124	-3.118 [15]	0.1335	0.0025	-0.0023	6	+2
K ₂ O	-1.033	-1.325	-1.264	-1.255 [15]	0.0830	-0.0263	-0.0035	8	+1
K ₂ O ₂	-1.071	-1.386	-1.254	-1.282 [15]	(-1.297)	(-1.278)	(-1.303)	12	+1
KO ₂	-0.888	-1.160	-1.011	-0.983 [15]	-0.5450	-0.2690	-0.0490	10	+1
CaO	-2.973	-3.389	-3.357	-3.290 [15]	0.1057	-0.0332	-0.0222	6	+2
Rb ₂ O	-0.917	-1.228	-1.158	-1.171 [15]	0.0950	-0.0215	0.0049	8	+1

TABLE A.XVI. (*continued*)

formula	PBE	LDA	SCAN	Exp.	$\delta H_{A-O}^{A+\alpha}$ PBE	$\delta H_{A-O}^{A+\alpha}$ LDA	$\delta H_{A-O}^{A+\alpha}$ SCAN	N_{A-O}	$+\alpha$
SrO	-2.744	-3.126	-3.115	-3.068 [15]	0.1082	-0.0192	-0.0155	6	+2
SrO ₂	-1.898	-2.313	-2.174	-2.189 [15]	(-2.228)	(-2.210)	(-2.203)	10	+2
Cs ₂ O	-0.994	-1.309	-1.205	-1.195 [15]	0.1008	-0.0567	-0.0050	6	+1
CsO ₂	-0.890	-1.168	-1.003	-0.989 [15]	(-1.045)	(-0.889)	(-0.970)	10	+1
BaO	-2.486	-2.811	-2.828	-2.841 [15]	0.1183	0.0098	0.0042	6	+2
BaO ₂	-1.860	-2.250	-2.123	-2.191 [15]	(-2.223)	(-2.244)	(-2.217)	10	+2
B ₂ O ₃	-2.406	-2.723	-2.696	-2.640 [15]	0.1952	-0.0693	-0.0472	6	+3
Al ₂ O ₃	-3.025	-3.491	-3.503	-3.473 [15]	0.1869	-0.0073	-0.0124	12	+3
SiO ₂ (α -qua.)	-2.810	-3.178	-3.175	-3.147 [15]	0.2530	-0.0233	-0.0208	4	+4
SiO ₂ (α -crist.)	-2.817	-3.167	-3.167	-3.138 [15]	(-3.154)	(-3.136)	(-3.139)	4	+4
Ga ₂ O ₃	-1.856	-2.244	-2.180	-2.258 [15]	0.2009	0.0068	0.0386	10	+3
GeO ₂	-1.605	-2.075	-1.924	-2.004 [15]	0.1992	-0.0357	0.0397	6	+4
As ₂ O ₅	-1.073	-1.453	-1.332	-1.362 [15]	0.2022	-0.0636	0.0212	10	+5
SeO ₂	-0.703	-1.005	-0.874	-0.778 [15]	0.0750	-0.2277	-0.0963	3	+4
In ₂ O ₃	-1.595	-1.959	-1.950	-1.919 [15]	0.1353	-0.0167	-0.0130	12	+3
SnO	-1.347	-1.609	-1.507	-1.481 [17]	0.0670	-0.0638	-0.0130	4	+2
SnO ₂	-1.706	-2.099	-2.037	-2.007 [17]	0.1505	-0.0460	-0.0153	6	+4
Sb ₂ O ₃	-1.340	-1.621	-1.508	-1.484 [15]	0.1207	-0.1135	-0.0198	6	+3
SbO ₂	-1.385	-1.764	-1.627	-1.567 [15]	(-1.571)	(-1.556)	(-1.557)	5	+3, +5
Sb ₂ O ₅	-1.259	-1.666	-1.537	-1.439 [17]	0.1052	-0.1323	-0.0573	12	+5
TeO ₂	-1.033	-1.388	-1.235	-1.117 [17]	0.0630	-0.2033	-0.0885	4	+4
Tl ₂ O	-0.591	-0.711	-0.701	-0.578 [15]	-0.0065	-0.0665	-0.0612	6	+1
Tl ₂ O ₃	-0.681	-1.034	-0.843	-0.809 [15]	0.0536	-0.0936	-0.0140	12	+3
PbO	-1.131	-1.355	-1.246	-1.137 [15]	0.0028	-0.1088	-0.0548	4	+2
Pb ₃ O ₄	-1.056	-1.311	-1.182	-1.064 [15]	(-1.107)	(-1.111)	(-1.113)	12	+2, +4
PbO ₂	-0.835	-1.198	-0.998	-0.948 [15]	0.0568	-0.1250	-0.0250	6	+4
Bi ₂ O ₃	-1.235	-1.533	-1.254	-1.183 [15]	-0.02580	-0.1752	-0.0356	10	+3
Sc ₂ O ₃	-3.567	-3.976	-4.017	-3.956 [15]	0.1618	-0.0083	-0.0257	12	+3
TiO	-2.541	-2.973	-2.876	-2.812 [15]	0.1131	-0.0667	-0.0265	4.8	+2
Ti ₂ O ₃	-2.917	-3.358	-3.318	-3.153 [15]	0.0980	-0.0855	-0.0688	12	+3
Ti ₃ O ₅	-2.975	-3.373	-3.375	-3.186 [15]	(-3.202)	(-3.172)	(-3.179)	18	+3, +4
TiO ₂ (rut.)	-3.047	-3.454	-3.509	-3.261 [15]	0.1072	-0.0965	-0.1237	6	+4
TiO ₂ (ana.)	-3.078	-3.464	-3.517	-3.243 [16]	(-3.293)	(-3.271)	(-3.270)	6	+4
VO	-1.446	-1.877	-1.767	-2.237 [15]	0.2637	0.1203	0.1568	6	+2
V ₂ O ₃	-2.290	-2.685	-2.654	-2.526 [15]	0.0984	-0.0661	-0.0531	12	+3
VO ₂	-2.373	-2.765	-2.773	-2.466 [15]	0.0467	-0.1497	-0.1537	6	+4
V ₂ O ₅	-2.307	-2.598	-2.607	-2.295 [15]	-0.0082	-0.2118	-0.2179	10	+5
Cr ₂ O ₃	-1.985	-2.243	-2.397	-2.352 [15]	0.1528	0.0454	-0.0189	12	+3
CrO ₃	-1.653	-1.826	-1.802	-1.521 [15]	-0.1323	-0.3053	-0.2813	4	+6
MnO	-1.240	-1.185	-2.092	-1.994 [15]	0.2513	0.2700	-0.0325	6	+2
MnO ₂	-1.680	-1.988	-2.116	-1.800 [15]	0.0600	-0.0943	-0.1582	6	+4
FeO	-0.881	-1.017	-1.353	-1.410 [16]	0.1763	0.1310	0.0188	6	+2
Fe ₂ O ₃	-1.315	-1.676	-1.864	-1.707 [15]	0.1633	0.0130	-0.0655	12	+3
CoO	-0.513	-0.734	-0.863	-1.232 [15]	0.2397	0.1662	0.1230	6	+2
NiO	-0.474	-0.776	-0.648	-1.242 [15]	0.2558	0.1552	0.1980	6	+2
Cu ₂ O	-0.415	-0.544	-0.505	-0.590 [16]	0.1310	0.0340	0.0635	4	+1
CuO	-0.606	-0.860	-0.795	-0.808 [16]	0.1015	-0.0258	0.0068	4	+2
ZnO	-1.446	-1.732	-1.726	-1.817 [15]	0.1853	0.0423	0.0455	4	+2
Y ₂ O ₃	-3.623	-4.001	-4.065	-3.949 [15]	0.1358	-0.0219	-0.0483	12	+3
ZrO ₂	-3.466	-3.897	-3.939	-3.791 [16]	0.1393	-0.0451	-0.0631	7	+4
NbO	-2.057	-2.428	-2.344	-2.175 [15]	0.0593	-0.1263	-0.0845	4	+2
MoO ₂	-1.973	-2.400	-2.242	-2.031 [15]	0.0292	-0.1843	-0.1053	6	+4
MoO ₃	-1.978	-2.272	-2.187	-1.931 [15]	-0.0470	-0.3410	-0.2558	4	+6
RuO ₂	-1.063	-1.465	-1.277	-1.054 [15]	-0.0048	-0.2057	-0.1118	6	+4
Rh ₂ O ₃	-0.703	-1.064	-0.877	-0.737 [15]	0.0141	-0.1363	-0.0583	12	+3
PdO	-0.483	-0.757	-0.647	-0.599 [15]	0.0578	-0.0793	-0.0245	4	+2
Ag ₂ O	-0.118	-0.179	-0.194	-0.107 [15]	-0.0083	-0.0540	-0.0653	4	+1
CdO	-1.026	-1.290	-1.323	-1.339 [15]	0.1042	0.0162	0.0053	6	+2
HfO ₂	-3.577	-4.024	-4.017	-3.955 [17]	0.1617	-0.0296	-0.0269	7	+4
WO ₂	-1.923	-2.354	-2.133	-2.037 [15]	0.0567	-0.1587	-0.0483	6	+4
WO ₃	-2.176	-2.495	-2.388	-2.183 [15]	0.0050	-0.2078	-0.1362	6	+6

TABLE A.XVI. (*continued*)

formula	PBE	LDA	SCAN	Exp.	$\delta H_{A-O}^{A+\alpha}$ PBE	$\delta H_{A-O}^{A+\alpha}$ LDA	$\delta H_{A-O}^{A+\alpha}$ SCAN	N_{A-O}	$+ \alpha$
ReO ₂	-1.372	-1.799	-1.509	-1.551 [17]	0.0897	-0.1242	0.0212	6	+4
ReO ₃	-1.635	-1.982	-1.766	-1.526 [17]	-0.0727	-0.3040	-0.1597	6	+6
OsO ₂	-0.894	-1.306	-1.015	-1.018 [15]	0.0617	-0.1443	0.0012	6	+4
OsO ₄	-0.994	-1.119	-1.038	-0.816 [15]	-0.2225	-0.3793	-0.2773	4	+8
IrO ₂	-0.798	-1.201	-0.802	-0.838 [17]	0.0202	-0.1813	0.0180	6	+4
HgO	-0.300	-0.535	-0.412	-0.470 [15]	0.1700	-0.0650	0.0580	2	+2

TABLE A.XVII: Formation energies and CCE corrections for binary halides. DFT formation energies (without vibrational contribution) and experimental room temperature formation enthalpies, corrections per bond $\delta H_{A-X}^{A+\alpha}$, number of cation-anion bonds N_{A-X} per formula unit and oxidation states $+ \alpha$ of the cation for binary halides. Experimental values from Kubaschewski *et al.* [15] and NIST-JANAF [16]. Note that BF₃ and SiF₄ are gaseous molecular systems. Energies and enthalpies in eV/atom; corrections in eV/bond.

formula	PBE	LDA	SCAN	Exp.	$\delta H_{A-X}^{A+\alpha}$ PBE	$\delta H_{A-X}^{A+\alpha}$ LDA	$\delta H_{A-X}^{A+\alpha}$ SCAN	N_{A-X}	$+ \alpha$
LiF	-2.972	-3.176	-3.356	-3.197 [16]	0.0748	0.0070	-0.0532	6	+1
NaF	-2.739	-2.914	-3.133	-2.982 [16]	0.0807	0.0225	-0.0503	6	+1
KF	-2.736	-2.928	-3.094	-2.946 [16]	0.0702	0.0060	-0.0490	6	+1
BeF ₂	-3.280	-3.483	-3.721	-3.547 [15]	0.2008	0.0480	-0.1300	4	+2
BF ₃ (g)	-2.786	-2.850	-3.092	-2.943 [15]	0.2093	0.1247	-0.1987	3	+3
AlF ₃	-3.560	-3.851	-4.118	-3.913 [15]	0.2353	0.0415	-0.1367	6	+3
SiF ₄ (g)	-3.121	-3.232	-3.494	-3.348 [15]	0.2833	0.1450	-0.1825	4	+4
NaCl	-1.840	-1.970	-2.086	-2.131 [15]	0.0972	0.0537	0.0152	6	+1
KCl	-1.988	-2.124	-2.220	-2.263 [15]	0.0913	0.0460	0.0142	6	+1
CaCl ₂	-2.436	-2.611	-2.713	-2.747 [15]	0.1552	0.0680	0.0167	6	+2
AlCl ₃	-1.551	-1.768	-1.770	-1.828 [15]	0.1845	0.0400	0.0388	6	+3

TABLE A.XVIII: Uncorrected and CCE corrected formation energies for ternary oxides. DFT formation energies (without vibrational contribution), coordination corrected values (using corrections from Table A.XVI) and experimental room temperature formation enthalpies, number of cation-oxygen bonds $N_{1/2-O}$ per formula unit and oxidation states $+ \alpha$ of the cations for ternary oxides. For the cation-oxygen bonds- and oxidation numbers, the first (second) number in the column refers to the first (second) element in the formula. Experimental values from Kubaschewski *et al.* [15], NIST-JANAF [16] and Barin [17]. Energies and enthalpies in eV/atom.

formula	PBE	LDA	SCAN	PBE CCE	LDA CCE	SCAN CCE	Exp.	$N_{1/2-O}$	$+ \alpha$
Ag ₂ CrO ₄	-1.100	-1.284	-1.300	-1.013	-1.032	-1.046	-1.083 [17]	10, 4	+1, +6
Al ₂ SiO ₅ (kya.)	-2.937	-3.388	-3.386	-3.343	-3.365	-3.357	-3.361 [16]	12, 4	+3, +4
Al ₂ SiO ₅ (and.)	-2.956	-3.373	-3.383	-3.339	-3.351	-3.356	-3.358 [16]	11, 4	+3, +4
BaAl ₂ O ₄	-3.064	-3.403	-3.483	-3.405	-3.405	-3.473	-3.441 [15]	7.5, 8	+2, +3
BaMoO ₄	-2.613	-2.871	-2.874	-2.739	-2.657	-2.709	-2.674 [17]	8, 4	+2, +6
BaTiO ₃	-3.090	-3.528	-3.540	-3.503	-3.436	-3.402	-3.441 [17]	12, 6	+2, +4
BaZrO ₃	-3.301	-3.697	-3.745	-3.752	-3.666	-3.679	-3.689 [17]	12, 6	+2, +4
BeAl ₂ O ₄	-2.970	-3.405	-3.419	-3.402	-3.397	-3.401	-3.407 [15]	4, 12	+2, +3
Be ₂ SiO ₄	-2.794	-3.179	-3.175	-3.162	-3.175	-3.170	-3.134 [16]	8, 4	+2, +4
CaAl ₄ O ₇	-3.074	-3.425	-3.492	-3.367	-3.402	-3.466	-3.477 [17]	5, 16	+2, +3
CaMoO ₄	-2.598	-2.922	-2.892	-2.707	-2.650	-2.692	-2.671 [15]	8, 4	+2, +6
Ca ₃ SiO ₅	-3.007	-3.403	-3.388	-3.331	-3.327	-3.334	-3.373 [15]	18, 4	+2, +4
CaSiO ₃ (wol.)	-3.047	-3.423	-3.421	-3.383	-3.363	-3.376	-3.389 [15]	6.3, 4	+2, +4
CaSiO ₃ (ps-wol.)	-3.026	-3.401	-3.404	-3.398	-3.330	-3.352	-3.375 [15]	8, 4	+2, +4
CaTiO ₃	-3.173	-3.604	-3.621	-3.470	-3.435	-3.437	-3.442 [15]	8, 6	+2, +4
Ca ₂ V ₂ O ₇	-2.810	-3.127	-3.160	-2.928	-2.914	-2.955	-2.905 [15]	13, 9	+2, +5
CaV ₂ O ₆	-2.647	-2.926	-2.959	-2.708	-2.669	-2.702	-2.682 [15]	6, 10	+2, +5
CaWO ₄	-2.662	-2.987	-2.960	-2.806	-2.804	-2.840	-2.842 [17]	8, 4	+2, +6
CaZrO ₃	-3.335	-3.734	-3.766	-3.629	-3.640	-3.664	-3.662 [15]	6, 6	+2, +4
CdAl ₂ O ₄	-2.443	-2.841	-2.846	-2.823	-2.838	-2.827	-2.838 [15]	4, 12	+2, +3
CdGa ₂ O ₄	-1.646	-2.002	-1.953	-2.050	-2.023	-2.022	-2.007 [15]	4, 12	+2, +3
CdTiO ₃	-2.291	-2.634	-2.683	-2.545	-2.537	-2.541	-2.551 [17]	6, 6	+2, +4
CoFe ₂ O ₄	-1.144	-1.465	-1.593	-1.561	-1.582	-1.551	-1.612 [15]	4, 12	+2, +3
CoTiO ₃	-2.097	-2.431	-2.499	-2.513	-2.515	-2.498	-2.503 [15]	6, 6	+2, +4

TABLE A.XVIII. (*continued*)

formula	PBE	LDA	SCAN	PBE CCE	LDA CCE	SCAN CCE	Exp.	$N_{1/2-O}$	+ α
CuFeO ₂	-0.925	-1.281	-1.325	-1.236	-1.318	-1.258	-1.329 [15]	2, 6	+1, +3
FeAl ₂ O ₄	-2.411	-2.753	-2.843	-2.832	-2.815	-2.832	-2.954 [17]	4, 12	+2, +3
FeMoO ₄	-1.643	-2.044	-2.065	-1.788	-1.948	-1.913	-1.831 [15]	6, 4	+2, +6
FeTiO ₃	-2.238	-2.520	-2.707	-2.579	-2.561	-2.581	-2.565 [15]	6, 6	+2, +4
LiAlO ₂	-2.738	-3.123	-3.132	-3.133	-3.088	-3.096	-3.080 [15]	6, 6	+1, +3
Li ₃ AsO ₄	-1.946	-2.209	-2.198	-2.162	-2.154	-2.191	-2.205 [17]	12, 4	+1, +5
Li ₂ SiO ₃	-2.561	-2.867	-2.866	-2.832	-2.831	-2.836	-2.848 [15]	8, 4	+1, +4
Li ₂ TiO ₃	-2.668	-3.005	-3.025	-2.929	-2.878	-2.878	-2.884 [15]	12, 6	+1, +4
Li ₂ ZrO ₃	-2.768	-3.088	-3.112	-3.061	-3.012	-3.025	-3.044 [15]	12, 6	+1, +4
MgAl ₂ O ₄	-2.991	-3.411	-3.434	-3.388	-3.400	-3.411	-3.404 [16]	4, 12	+2, +3
MgCr ₂ O ₄	-2.231	-2.468	-2.629	-2.569	-2.547	-2.595	-2.632 [15]	4, 12	+2, +3
MgMoO ₄	-2.375	-2.640	-2.633	-2.477	-2.416	-2.460	-2.419 [15]	6, 4	+2, +6
Mg ₂ SiO ₄	-2.838	-3.218	-3.230	-3.211	-3.209	-3.214	-3.223 [15]	12, 4	+2, +4
MgSiO ₃	-2.826	-3.220	-3.222	-3.189	-3.205	-3.203	-3.210 [15]	6, 4	+2, +4
MgTiO ₃	-2.983	-3.372	-3.413	-3.272	-3.259	-3.262	-3.260 [15]	6, 6	+2, +4
MgTi ₂ O ₅	-3.029	-3.402	-3.451	-3.289	-3.259	-3.264	-3.251 [16]	6, 12	+2, +4
MgV ₂ O ₆	-2.487	-2.796	-2.817	-2.566	-2.563	-2.573	-2.534 [15]	6, 10	+2, +5
Mg ₂ V ₂ O ₇	-2.581	-2.878	-2.922	-2.721	-2.726	-2.761	-2.671 [15]	12, 8	+2, +5
MgWO ₄	-2.450	-2.806	-2.756	-2.588	-2.601	-2.618	-2.621 [15]	6, 6	+2, +6
MnTiO ₃	-2.447	-2.648	-3.052	-2.877	-2.856	-2.865	-2.817 [15]	6, 6	+2, +4
NaCrO ₂	-1.905	-2.127	-2.296	-2.258	-2.188	-2.251	-2.271 [15]	6, 6	+1, +3
Na ₂ CrO ₄	-1.979	-2.186	-2.215	-2.021	-2.005	-2.038	-1.987 [17]	10, 4	+1, +6
NaFeO ₂	-1.554	-1.717	-1.944	-1.799	-1.726	-1.867	-1.809 [15]	4, 4	+1, +3
Na ₂ MoO ₄	-2.123	-2.352	-2.364	-2.238	-2.149	-2.198	-2.175 [17]	12, 4	+1, +6
Na ₄ SiO ₄	-2.098	-2.381	-2.406	-2.375	-2.362	-2.374	-2.420 [15]	18, 4	+1, +4
Na ₂ SiO ₃	-2.369	-2.667	-2.687	-2.674	-2.644	-2.655	-2.700 [15]	10, 4	+1, +4
Na ₂ Ti ₃ O ₇	-2.796	-3.128	-3.178	-3.016	-2.988	-2.993	-3.007 [15]	10, 17	+1, +4
NaVO ₃	-2.350	-2.563	-2.626	-2.442	-2.389	-2.439	-2.379 [17]	6, 4	+1, +5
Na ₂ WO ₄	-2.175	-2.399	-2.419	-2.319	-2.273	-2.322	-2.283 [15]	12, 4	+1, +6
NiAl ₂ O ₄	-2.289	-2.654	-2.672	-2.755	-2.730	-2.764	-2.844 [15]	4, 12	+2, +3
NiTiO ₃	-2.077	-2.408	-2.406	-2.513	-2.479	-2.495	-2.492 [15]	6, 6	+2, +4
NiWO ₄	-1.661	-1.984	-1.889	-1.922	-1.931	-1.951	-1.950 [15]	6, 6	+2, +6
PbMoO ₄	-1.888	-2.131	-2.063	-1.861	-1.759	-1.819	-1.819 [15]	8, 4	+2, +6
PbTiO ₃	-2.346	-2.684	-2.654	-2.458	-2.413	-2.443	-2.476 [15]	8, 5	+2, +4
PbWO ₄	-1.944	-2.184	-2.121	-1.950	-1.900	-1.957	-1.937 [15]	8, 4	+2, +6
SrAl ₂ O ₄	-3.077	-3.424	-3.494	-3.383	-3.399	-3.466	-3.442 [17]	6, 8	+2, +3
SrHfO ₃	-3.415	-3.827	-3.844	-3.782	-3.760	-3.787	-3.697 [15]	8, 6	+2, +4
SrMoO ₄	-2.624	-2.920	-2.906	-2.737	-2.667	-2.715	-2.676 [15]	8, 4	+2, +6
SrSiO ₃	-3.040	-3.405	-3.414	-3.415	-3.355	-3.372	-3.386 [15]	8, 4	+2, +4
Sr ₂ TiO ₄	-3.075	-3.495	-3.508	-3.445	-3.363	-3.363	-3.387 [15]	18, 6	+2, +4
SrTiO ₃	-3.168	-3.603	-3.628	-3.556	-3.441	-3.442	-3.463 [15]	12, 6	+2, +4
SrWO ₄	-2.686	-2.981	-2.972	-2.833	-2.817	-2.861	-2.832 [17]	8, 4	+2, +6
ZnFe ₂ O ₄	-1.284	-1.678	-1.788	-1.670	-1.725	-1.702	-1.735 [17]	4, 12	+2, +3
Zn ₂ SiO ₄	-2.057	-2.382	-2.376	-2.414	-2.417	-2.416	-2.433 [15]	8, 4	+2, +4
Zn ₂ TiO ₄	-2.120	-2.465	-2.487	-2.476	-2.442	-2.446	-2.443 [15]	10, 6	+2, +4
ZnWO ₄	-1.939	-2.286	-2.217	-2.129	-2.120	-2.127	-2.126 [15]	6, 6	+2, +6
ZrSiO ₄	-3.156	-3.592	-3.600	-3.510	-3.517	-3.502	-3.496 [16]	8, 4	+4, +4

TABLE A.XIX: Uncorrected and CCE corrected formation energies for ternary halides. DFT formation energies (without vibrational contribution), coordination corrected values (using corrections from Table A.XVII) and experimental room temperature formation enthalpies, number of cation-anion bonds $N_{1/2-X}$ per formula unit and oxidation states $+ $\alpha$$ of the cations for ternary halides. For the cation-oxygen bonds- and oxidation numbers, the first (second) number in the column refers to the first (second) element in the formula. Experimental values from Kubaschewski *et al.* [15] and NIST-JANAF [16]. Energies and enthalpies in eV/atom.

formula	PBE	LDA	SCAN	PBE CCE	LDA CCE	SCAN CCE	Exp.	$N_{1/2-X}$	+ α
KBF ₄	-3.040	-3.243	-3.433	-3.297	-3.336	-3.219	-3.255 [15]	10, 4	+1, +3
Li ₃ AlF ₆	-3.246	-3.462	-3.682	-3.487	-3.496	-3.529	-3.507 [16]	13.3, 6	+1, +3
Li ₂ BeF ₄	-3.145	-3.310	-3.524	-3.345	-3.346	-3.389	-3.365 [15]	8, 4	+1, +2
Na ₃ AlF ₆	-3.090	-3.280	-3.520	-3.360	-3.341	-3.358	-3.433 [15]	16, 6	+1, +3

TABLE A.XIX. (*continued*)

formula	PBE	LDA	SCAN	PBE CCE	LDA CCE	SCAN CCE	Exp.	$N_{1/2-X}$	+ α
NaBF ₄	-2.969	-3.162	-3.360	-3.216	-3.275	-3.161	-3.187 [15]	8, 4	+1, +3
Na ₂ SiF ₆	-3.103	-3.333	-3.535	-3.399	-3.459	-3.346	-3.354 [15]	12, 6	+1, +4
NaAlCl ₄	-1.707	-1.828	-1.916	-1.911	-1.899	-1.955	-1.973 [16]	5, 4	+1, +3

- [1] S. Curtarolo, G. L. W. Hart, M. Buongiorno Nardelli, N. Mingo, S. Sanvito, and O. Levy, *The high-throughput highway to computational materials design*, Nat. Mater. **12**, 191–201 (2013).
- [2] C. Wolverton and V. Ozoliņš, *First-principles aluminum database: Energetics of binary Al alloys and compounds*, Phys. Rev. B **73**, 144104 (2006).
- [3] S. Curtarolo, D. Morgan, and G. Ceder, *Accuracy of ab initio methods in predicting the crystal structures of metals: A review of 80 binary alloys*, Calphad **29**, 163–211 (2005).
- [4] W. Kohn and L. J. Sham, *Self-consistent equations including exchange and correlation effects*, Phys. Rev. **140**, A1133 (1965).
- [5] U. von Barth and L. Hedin, *A local exchange-correlation potential for the spin polarized case: I*, J. Phys. C: Solid State Phys. **5**, 1629 (1972).
- [6] J. P. Perdew, K. Burke, and M. Ernzerhof, *Generalized Gradient Approximation Made Simple*, Phys. Rev. Lett. **77**, 3865–3868 (1996).
- [7] C. Osés, C. Toher, and S. Curtarolo, *Data-driven design of inorganic materials with the Automatic Flow Framework for Materials Discovery*, MRS Bull. **43**, 670–675 (2018).
- [8] W. Setyawan and S. Curtarolo, *High-throughput electronic band structure calculations: Challenges and tools*, Comput. Mater. Sci. **49**, 299–312 (2010).
- [9] R. H. Taylor, F. Rose, C. Toher, O. Levy, K. Yang, M. Buongiorno Nardelli, and S. Curtarolo, *A RESTful API for exchanging materials data in the AFLOWLIB.org consortium*, Comput. Mater. Sci. **93**, 178–192 (2014).
- [10] F. Rose, C. Toher, E. Gossett, C. Osés, M. Buongiorno Nardelli, M. Fornari, and S. Curtarolo, *AFLUX: The LUX materials search API for the AFLOW data repositories*, Comput. Mater. Sci. **137**, 362–370 (2017).
- [11] A. Jain, G. Hautier, C. J. Moore, S. P. Ong, C. C. Fischer, T. Mueller, K. A. Persson, and G. Ceder, *A high-throughput infrastructure for density functional theory calculations*, Comput. Mater. Sci. **50**, 2295–2310 (2011).
- [12] A. Jain, S. P. Ong, G. Hautier, W. Chen, W. D. Richards, S. Dacek, S. Cholia, D. Gunter, D. Skinner, G. Ceder, and K. A. Persson, *Commentary: The Materials Project: A materials genome approach to accelerating materials innovation*, APL Mater. **1**, 011002 (2013).
- [13] J. E. Saal, S. Kirklin, M. Aykol, B. Meredig, and C. Wolverton, *Materials Design and Discovery with High-Throughput Density Functional Theory: The Open Quantum Materials Database (OQMD)*, JOM **65**, 1501–1509 (2013).
- [14] S. Kirklin, J. E. Saal, B. Meredig, A. Thompson, J. W. Doak, M. Aykol, S. Rühl, and C. Wolverton, *The Open Quantum Materials Database (OQMD): assessing the accuracy of DFT formation energies*, NPJ Comput. Mater. **1**, 15010 (2015).
- [15] O. Kubaschewski, C. B. Alcock, and P. J. Spencer, *Materials Thermochemistry* (Pergamon Press, Oxford, UK, 1993), 6th edn.
- [16] M. W. Chase, *NIST-JANAF Thermochemical Tables* (American Chemical Society and American Institute of Physics for the National Institute of Standards and Technology, Woodbury, NY, 1998), 4th edn.
- [17] I. Barin, *Thermochemical Data of Pure Substances* (VCH, Weinheim, 1995), 3rd edn.
- [18] D. D. Wagman, W. H. Evans, V. B. Parker, R. H. Schumm, I. Halow, S. M. Bailey, K. L. Churney, and R. L. Nuttall, *The NBS tables of chemical thermodynamic properties*, J. Phys. Chem. Ref. Data **11**, Supplement No. 2 (1982).
- [19] G. Hautier, S. P. Ong, A. Jain, C. J. Moore, and G. Ceder, *Accuracy of density functional theory in predicting formation energies of ternary oxides from binary oxides and its implication on phase stability*, Phys. Rev. B **85**, 155208 (2012).
- [20] R. Sarmiento-Pérez, S. Botti, and M. A. L. Marques, *Optimized Exchange and Correlation Semilocal Functional for the Calculation of Energies of Formation*, J. Chem. Theory Comput. **11**, 3844–3850 (2015).
- [21] V. L. Chevrier, S. P. Ong, R. Armiento, M. K. Y. Chan, and G. Ceder, *Hybrid density functional calculations of redox potentials and formation energies of transition metal compounds*, Phys. Rev. B **82**, 075122 (2010).
- [22] J. Sun, A. Ruzsinszky, and J. P. Perdew, *Strongly Constrained and Appropriately Normed Semilocal Density Functional*, Phys. Rev. Lett. **115**, 036402 (2015).
- [23] Y. Zhang, D. A. Kitcheev, J. Yang, T. Chen, S. T. Dacek, R. A. Sarmiento-Pérez, M. A. L. Marques, H. Peng, G. Ceder, J. P. Perdew, and J. Sun, *Efficient first-principles prediction of solid stability: Towards chemical accuracy*, NPJ Comput. Mater. **4**, 9 (2018).
- [24] E. B. Isaacs and C. Wolverton, *Performance of the strongly constrained and appropriately normed density functional for solid-state materials*, Phys. Rev. Mater. **2**, 063801 (2018).
- [25] J. Yan, J. S. Hummelshøj, and J. K. Nørskov, *Formation energies of group I and II metal oxides using random phase approximation*, Phys. Rev. B **87**, 075207 (2013).
- [26] J. Yan and J. K. Nørskov, *Calculated formation and reaction energies of 3d transition metal oxides using a hierarchy of exchange-correlation functionals*, Phys. Rev. B **88**, 245204 (2013).
- [27] T. S. Jauho, T. Olsen, T. Bligaard, and K. S. Thygesen, *Improved description of metal oxide stability: Beyond the random phase approximation with renormalized kernels*, Phys. Rev. B **92**, 115140 (2015).

- [28] M. Pandey and K. W. Jacobsen, *Heats of formation of solids with error estimation: The mBEEF functional with and without fitted reference energies*, Phys. Rev. B **91**, 235201 (2015).
- [29] L. Wang, T. Maxisch, and G. Ceder, *Oxidation energies of transition metal oxides within the GGA+U framework*, Phys. Rev. B **73**, 195107 (2006).
- [30] S. Grindly, B. Meredig, S. Kirklin, J. E. Saal, and C. Wolverton, *Approaching chemical accuracy with density functional calculations: Diatomic energy corrections*, Phys. Rev. B **87**, 075150 (2013).
- [31] Y. Yu, M. Aykol, and C. Wolverton, *Reaction thermochemistry of metal sulfides with GGA and GGA+U calculations*, Phys. Rev. B **92**, 195118 (2015).
- [32] A. Jain, G. Hautier, S. P. Ong, C. J. Moore, C. C. Fischer, K. A. Persson, and G. Ceder, *Formation enthalpies by mixing GGA and GGA+U calculations*, Phys. Rev. B **84**, 045115 (2011).
- [33] M. Aykol and C. Wolverton, *Local environment dependent GGA+U method for accurate thermochemistry of transition metal compounds*, Phys. Rev. B **90**, 115105 (2014).
- [34] S. Lany, *Semiconductor thermochemistry in density functional calculations*, Phys. Rev. B **78**, 245207 (2008).
- [35] V. Stevanović, S. Lany, X. Zhang, and A. Zunger, *Correcting density functional theory for accurate predictions of compound enthalpies of formation: Fitted elemental-phase reference energies*, Phys. Rev. B **85**, 115104 (2012).
- [36] M. A. Blanco, A. M. Pendás, E. Francisco, J. M. Recio, and R. Franco, *Thermodynamical properties of solids from microscopic theory: Applications to MgF₂ and Al₂O₃*, J. Mol. Struct.: Theochim **368**, 245–255 (1996).
- [37] M. A. Blanco, E. Francisco, and V. Luaña, *GIBBS: isothermal-isobaric thermodynamics of solids from energy curves using a quasi-harmonic Debye model*, Comput. Phys. Commun. **158**, 57–72 (2004).
- [38] C. Toher, J. J. Plata, O. Levy, M. de Jong, M. D. Asta, M. Buongiorno Nardelli, and S. Curtarolo, *High-throughput computational screening of thermal conductivity, Debye temperature, and Grüneisen parameter using a quasiharmonic Debye model*, Phys. Rev. B **90**, 174107 (2014).
- [39] C. Toher, C. Oses, J. J. Plata, D. Hicks, F. Rose, O. Levy, M. de Jong, M. D. Asta, M. Fornari, M. Buongiorno Nardelli, and S. Curtarolo, *Combining the AFLOW GIBBS and elastic libraries to efficiently and robustly screen thermomechanical properties of solids*, Phys. Rev. Materials **1**, 015401 (2017).
- [40] J.-P. Poirier, *Introduction to the Physics of the Earth's Interior* (Cambridge University Press, 2000), 2nd edn.
- [41] K. Momma and F. Izumi, *VESTA3 for three-dimensional visualization of crystal, volumetric and morphology data*, J. Appl. Crystallogr. **44**, 1272–1276 (2011).
- [42] Y. Hinuma, H. Hayashi, Y. Kumagai, I. Tanaka, and F. Oba, *Comparison of approximations in density functional theory calculations: Energetics and structure of binary oxides*, Phys. Rev. B **96**, 094102 (2017).
- [43] P. W. Atkins and J. De Paula, *Atkins' Physical Chemistry* (W.H. Freeman,, New York, 2006), 8th edn.
- [44] G. Henkelman, A. Arnaldsson, and H. Jónsson, *A fast and robust algorithm for Bader decomposition of charge density*, Comput. Mater. Sci. **36**, 354–360 (2006).
- [45] C. Toher, C. Oses, D. Hicks, E. Gossett, F. Rose, P. Nath, D. Usanmaz, D. C. Ford, E. Perim, C. E. Calderon, J. J. Plata, Y. Lederer, M. Jahnátek, W. Setyawan, S. Wang, J. Xue, K. Rasch, R. V. Chepulskii, R. H. Taylor, G. Gomez, H. Shi, A. R. Supka, R. Al Rahal Al Orabi, P. Gopal, F. T. Cerasoli, L. Liyanage, H. Wang, I. Siloi, L. A. Agapito, C. Nyshadham, G. L. W. Hart, J. Carrete, F. Legrain, N. Mingo, E. Zurek, O. Isayev, A. Tropsha, S. Sanvito, R. M. Hanson, I. Takeuchi, M. J. Mehl, A. N. Kolmogorov, K. Yang, P. D'Amico, A. Calzolari, M. Costa, R. De Gennaro, M. Buongiorno Nardelli, M. Fornari, O. Levy, and S. Curtarolo, *The AFLOW Fleet for Materials Discovery*, in *Handbook of Materials Modeling*, edited by W. Andreoni and S. Yip (Springer International Publishing, Cham, Switzerland, 2018), pp. 1–28, doi:10.1007/978-3-319-42913-7_63-1.
- [46] C. H. P. Lupis, *Chemical Thermodynamics of Materials* (North-Holland, New York, 1983).
- [47] C. E. Calderon, J. J. Plata, C. Toher, C. Oses, O. Levy, M. Fornari, A. Natan, M. J. Mehl, G. L. W. Hart, M. Buongiorno Nardelli, and S. Curtarolo, *The AFLOW standard for high-throughput materials science calculations*, Comput. Mater. Sci. **108 Part A**, 233–238 (2015).
- [48] A. R. Supka, T. E. Lyons, L. S. I. Liyanage, P. D'Amico, R. Al Rahal Al Orabi, S. Mahatara, P. Gopal, C. Toher, D. Ceresoli, A. Calzolari, S. Curtarolo, M. Buongiorno Nardelli, and M. Fornari, *AFLOWπ: A minimalist approach to high-throughput ab initio calculations including the generation of tight-binding hamiltonians*, Comput. Mater. Sci. **136**, 76–84 (2017).
- [49] M. J. Mehl, D. Hicks, C. Toher, O. Levy, R. M. Hanson, G. L. W. Hart, and S. Curtarolo, *The AFLOW Library of Crystallographic Prototypes: Part 1*, Comput. Mater. Sci. **136**, S1–S828 (2017).
- [50] D. Hicks, M. J. Mehl, E. Gossett, C. Toher, O. Levy, R. M. Hanson, G. L. W. Hart, and S. Curtarolo, *The AFLOW Library of Crystallographic Prototypes: Part 2*, in press doi:10.1016/j.commatsci.2018.10.043 (2019).
- [51] G. Kresse and J. Hafner, *Ab initio molecular dynamics for liquid metals*, Phys. Rev. B **47**, 558–561 (1993).
- [52] G. Kresse and J. Furthmüller, *Efficient iterative schemes for ab initio total-energy calculations using a plane-wave basis set*, Phys. Rev. B **54**, 11169–11186 (1996).
- [53] G. Kresse and D. Joubert, *From ultrasoft pseudopotentials to the projector augmented-wave method*, Phys. Rev. B **59**, 1758–1775 (1999).
- [54] Springer Materials, <https://materials.springer.com>. (accessed November 20, 2018).
- [55] D. Hicks, C. Oses, E. Gossett, G. Gomez, R. H. Taylor, C. Toher, M. J. Mehl, O. Levy, and S. Curtarolo, *AFLOW-SYM: platform for the complete, automatic and self-consistent symmetry analysis of crystals*, Acta Crystallogr. Sect. A **74**, 184–203 (2018).
- [56] http://aflow.org/CrystalDatabase/A2B_hP9_152_c_a.html.
- [57] http://aflow.org/CrystalDatabase/A2B_tP12_92_b_a.html.
- [58] http://aflow.org/CrystalDatabase/A2B_tP6_136_f_a.html.
- [59] http://aflow.org/CrystalDatabase/A2B_tI12_141_e_a.html.
- [60] O. Levy, G. L. W. Hart, and S. Curtarolo, *Hafnium binary alloys from experiments and first principles*, Acta Mater. **58**, 2887–2897 (2010).
- [61] M. R. Pederson, A. Ruzsinszky, and J. P. Perdew, *Communication: Self-interaction correction with unitary invariance in density functional theory*, J. Chem. Phys. **140**,

- 121103 (2014).
- [62] Z.-h. Yang, M. R. Pederson, and J. P. Perdew, *Full self-consistency in the Fermi-orbital self-interaction correction*, Phys. Rev. A **95**, 052505 (2017).
- [63] D.-y. Kao, K. Withanage, T. Hahn, J. Batool, J. Kortus, and K. Jackson, *Self-consistent self-interaction corrected density functional theory calculations for atoms using Fermi-Löwdin orbitals: Optimized Fermi-orbital descriptors for Li-Kr*, J. Chem. Phys. **147**, 164107 (2017).
- [64] S. Schwalbe, T. Hahn, S. Liebing, K. Trepte, and J. Kortus, *Fermi-Löwdin Orbital Self-interaction Corrected Density Functional Theory: Ionization Potentials and Enthalpies of Formation*, J. Comput. Chem. **39**, 2463–2471 (2018).
- [65] The MAE of the quasi-FERE method on the test set is smaller than the one on the binary fit set for all functionals in agreement with previous results [35]. The fitting set contains a larger variety of elements in oxidation states potentially problematic for DFT. In the test set of ternary oxides there are fewer such cases leading to smaller MAEs.
- [66] J. P. Perdew, A. Ruzsinszky, G. I. Csonka, O. A. Vydrov, G. E. Scuseria, L. A. Constantin, X. Zhou, and K. Burke, *Restoring the Density-Gradient Expansion for Exchange in Solids and Surfaces*, Phys. Rev. Lett. **100**, 136406 (2008).
- [67] Z.-h. Yang, H. Peng, J. Sun, and J. P. Perdew, *More realistic band gaps from meta-generalized gradient approximations: Only in a generalized Kohn-Sham scheme*, Phys. Rev. B **93**, 205205 (2016).
- [68] F. Legrain, J. Carrete, A. van Roekeghem, S. Curtarolo, and N. Mingo, *How Chemical Composition Alone Can Predict Vibrational Free Energies and Entropies of Solids*, Chem. Mater. **29**, 6220–6227 (2017).
- [69] http://aflow.org/CrystalDatabase/AB_cF8_216_c_a.html.
- [70] http://aflow.org/CrystalDatabase/AB_tI4_119_c_a.html.
- [71] C. Osés, E. Gossett, D. Hicks, F. Rose, M. J. Mehl, E. Perim, I. Takeuchi, S. Sanvito, M. Scheffler, Y. Lederer, O. Levy, C. Toher, and S. Curtarolo, *AFLOW-CHUL: Cloud-Oriented Platform for Autonomous Phase Stability Analysis*, J. Chem. Inf. Model. **58**, 2477–2490 (2018).
- [72] P. Sarker, T. Harrington, C. Toher, C. Osés, M. Samiee, J.-P. Maria, D. W. Brenner, K. S. Vecchio, and S. Curtarolo, *High-entropy high-hardness metal carbides discovered by entropy descriptors*, Nat. Commun. **9**, 4980 (2018).
- [73] B. Hammer, L. B. Hansen, and J. K. Nørskov, *Improved adsorption energetics within density-functional theory using revised Perdew-Burke-Ernzerhof functionals*, Phys. Rev. B **59**, 7413–7421 (1999).